Multifunctional Silver-based Nanomaterials for Non-conventional Oral Cancer Therapy through Simultaneous LOX and Selective COX-2 inhibition

Multifunctional Silver-based Nanomaterials for Non-conventional Oral Cancer Therapy Through Simultaneous LOX and Selective COX-2 inhibition

Fiza ur Rehman[1,2], Syeda Sohaila Naz[2#], Muhammad Junaid Dar[3], Annum Malik[1], Maimoona Qindeel[4], Francesco Baino[5]**, Fazli Wahid[6], Abbas Rahdar [7# #], Saeeda Munir[8], Sara Qaiser[2], Kifayat Ullah Shah[1]*

1. Saulat Institute of Pharmaceutical Sciences, Quaid-i-Azam University, Islamabad, Pakistan.
2. Nanosciences and Technology Department, National Centre for Physics (NCP), Islamabad, Pakistan.
3. Department of Pharmacy, The University of Lahore, Islamabad, Pakistan.
4. Hamdard institute of Pharmaceutical Sciences, Hamdard University, Islamabad campus, Islamabad.
5. Institute of Materials Physics and Engineering, Applied Science and Technology Department, Politecnico di Torino, Torino, Italy.
6. COMSATS University, Abbotabad, Pakistan.
7. Deparment of Physics, University of Zabol, Zabol, Iran.
8. Institute of Biomedical and Genetic Engineering (IBGE), Islamabad, Pakistan.

Corresponding Authors

*Kifayat Ullah Shah kushah@qau.edu.pk

#Syeda Sohaila Naz organicsoul84@gmail.com

** Francesco Baino francesco.baino@polito.it

Abbas Rahdar a.rahdarnanophysics@gmail.com

Abstract

Neoplastic cells have co-opted inflammatory receptors and signaling molecules that potentiate inflammation. Activated inflammatory pathways lead to neo-angiogenesis, lymph-angiogenesis, immunosuppression, tumor growth, proliferation and metastasis. This cancer-sustaining inflammation is a critical target to arrest cancer growth. Multiple drug resistance, high cost, low oral bioavailability and serious side effects have rendered conventional cytotoxic chemotherapeutics less impressive. The aim of this research was to achieve cancer debulking and proliferation prevention by limiting 'cancer-sustaining' tumor niche inflammation through non-conventional oral approach employing anti-inflammatory agents and avoiding conventional cytotoxic agents. Synergistic anti-inflammatory agents, i.e. celecoxib as selective COX-2 inhibitor and montelukast as cysteinyl leukotriene receptor antagonist, were selected. Silver nanoparticles (AgNPs) were used as nanocarriers because of their efficient synergistic anti-neoplastic effects and excellent oral drug delivery potential. Specifically, selected drugs were co-conjugated onto AgNPs. Synthesized nanoparticles were then surface-modified with poly(vinyl alcohol) to control particle size, avoid opsonization/preferred cellular uptake and improve dispersion. Surface plasmon resonance analysis, particle size analysis, DSC, TGA, XRD, FTIR and LIBS analysis confirmed the successful conjugation of drugs and efficient polymer coating with high loading efficiency. *In-vitro,* the nanoparticles manifested best and sustained release in moderately acidic (pH 4.5) milieu enabling passive tumor targeting potential. *In-vivo*, synthesized nanoparticles exhibited efficient dose-dependent anti-inflammatory activity reducing the dose up to 25-fold. The formulation also manifested hemo-compatibility, potent anti-denaturation activity and dose-dependent *in-vitro* and *in-vivo* anti-cancer potential against MCF-7 breast cancer and Hep-G2 liver cancer cell lines in both orthotopic and subcutaneous xenograft cancer models. The anti-inflammatory nanoparticles manifested tumor specific release potential exhibiting selective cytotoxicity at cancerous milieu with slightly acidic environment and activated inflammatory pathways. The formulation displayed impressive oral bioavailability, sustained release, negligible cytotoxicity against THLE-2 normal human hepatocytes, low toxicity (high LD_{50}) and wide therapeutic window. Results suggest promise of developed nanomaterials as hemo-compatible, potent, cheaper, less-toxic oral anti-inflammatory and non-conventional anti-cancer agents.

Keywords: Nanoparticles; Anti-cancer; Anti-inflammatory; Non-conventional chemotherapy; Drug delivery.

1. Introduction

Cancer has a substantial impact on society, worldwide. It has become the 2nd leading cause of death with 9.6 million deaths in 2018, globally [1]. There is a flustering rise in cancer prevalence and it is expected to rise to 23.6 and 27.5 million new cases per year by 2030 and 2040, respectively [2, 3]. The overall economic impact of the problem is tremendous showing a persistent upsurge. The suffering is more pronounced in middle- and low-income countries with estimated 70 % mortality rate [1, 2]. Advanced research in the field is addressed to mitigate some existing limitations, including serious side effects, high price and drug resistance associated with traditional chemotherapeutics along with tumor relapse [4-7].

Cancer stem cells orchestrate 'tumor niche' for their function, survival, growth and proliferation. This tumor microenvironment comprises inflammatory cells, non-epithelial stromal cells and vasculature [8, 9]. Neoplastic cells with co-opted inflammatory surface receptors produce signaling molecules including mitogenic chemokines and cytokines which potentiate inflammation [9, 10]. Inflammatory factors then lead to neo-angiogenesis, lymph-angiogenesis, tumor growth, immunosuppression, proliferation and metastasis [11-16]. Moreover, chronic inflammation can lead to mutations, epigenetic alterations and DNA damage, converting normal cells into cancer cells [17-19]. Therefore, inflammatory cells of tumor niche are critical targets to arrest cancer growth. Chronic inflammation is also linked to hay fever, osteoarthritis, inflammatory bowel disease, atherosclerosis, periodontal diseases, microbial infections and AIDS [20-24]. Managing inflammation can, therefore, play influential roles in suppressing such distressing conditions and avoiding cancer development.

Inflammatory pathways include cyclooxygenase and lipooxygenase pathways involving cyclooxygenase (COX) and 5-lipooxygenase (5-LOX) enzymes. COX exists in COX-1 (constitutive) and COX-2 (inducible) isoforms [25]. COX-1 is involved in maintenance of platelet aggregation, renal perfusion and mucosal protection, whereas, COX-2 is involved in inflammation and cell proliferation [25, 26]. COX-2 expression is upregulated in cancer, producing vascular endothelial growth factor (VEGF) and

prostaglandins, hence, playing a key role in tumor niche development. Inhibition of COX-2 can not only impede cancer growth and regress tumor mass but also reduces cancer incidence [27, 28]. However, selective COX-2 inhibitors increase cardiovascular risk promoting thrombotic events which might be attributed to disturbance in prostacyclin/thromboxane balance. Moreover, the associated side effects are dose related, therefore, reducing the dose can possibly, alleviate associated risks [29-34]. There is also clear evidence indicating the over-expression of 5-LOX and leukotriene receptors in colon, prostate, lung, breast, head and neck cancers [35-40]. Some studies demonstrated that 5-LOX inhibition initiates apoptosis of neoplastic cells leading to tumor mass regression [37, 38, 40]. Anti-cancer potential, lower cost and very low toxicity profile (in comparison to conventional chemotherapeutics) provide a strong rationale for the use of COX-2 and 5-LOX inhibitors in chemotherapy [41, 42].

Silver nanoparticles (AgNPs), due to their unique properties, are widely employed in biomedical applications. They have shown vast potential as anti-microbial, anti-inflammatory, anti-angiogenic and anti-cancer agents [43-45]. These effects can be attributed to their ability of generating ROS, thus damaging DNA, cell membrane and inducing mitochondrial and nuclear disruption through oxidative stress and apoptosis or necrosis enforcement capabilities [43-48]. Potential for optical imaging, heat-based targeted therapy, diagnostics, dense surface ligand functionalization, high aqueous solubility, sustained drug release potential and larger specific surface area render them ideal platforms for local treatment and controlled drug delivery [44-48]. However, AgNPs are associated with size-dependent toxicity risk [49, 50]. Polymer encapsulation of AgNPs is an efficient technique to control particle size and hence toxicity [51, 52]. Surface modification with hydrophilic polymers can also provide chemical stability, improved solubility and dispersion, biocompatibility, reduced toxicity and protection from reticulo-endothelial system (RES) [53, 54]. Poly(vinyl alcohol) (PVA), a non-toxic, hydrophilic and biodegradable polymer promotes cellular uptake of nanoparticles by imparting slight negative surface charge [52, 55-60].

In the present study, in order to refine the anti-cancer treatment by exploring better therapeutic alternatives (e.g. oral, non-toxic, potent, safe and cheaper prospects) to more toxic conventional cytotoxic drugs, anti-inflammatory agents were selected for cancer debulking and proliferation prevention of tumor cells. The idea was to impair 'cancer-sustaining' inflammatory cells in the tumor niche and impede inflammation along with reducing the proliferation of neoplastic cells, simultaneously. Silver nanoparticles were preferred to other nano-metals as nanocarriers for selected anti-inflammatory agents because of their efficient synergistic anti-neoplastic effects along with excellent oral drug delivery potential. Oral delivery of non-conventional anti-cancer agents and avoiding cytotoxicity to normal cells was focused. The strategy was to avoid toxic anti-cancer agents which attack both cancerous and normal cells. Most of these agents are administered intravenously and their oral delivery is a challenge in itself.

Celecoxib (CX), a selective COX-2 inhibitor (NSAID) and montelukast (MKT), a cysteinyl leukotriene (cysLT) receptor antagonist, were selected because of their potent selective anti-inflammatory, anti-angiogenic and anti-cancer activities [27, 28, 38, 40, 61-65]. Celecoxib cannot only vanquish inflammation along with avoiding gastrointestinal side effects by inhibiting COX-2 selectively, but also exerts inflammation independent anti-cancer effects. It blocks PDK-1 (3-phosphoinositide-dependent kinase-1) signaling mechanism, binds to tumor assisting CDH11 (cadherin-11) protein, and inhibits carbonic anhydrase 2 and 3 enzymes, thus arresting cancer progression [61, 62, 64]. cysLT receptor blocker was preferred over 5-LOX inhibitor. This is because 5-LOX inhibitors also inhibit the biosynthesis of lipoxins, which display pro-resolution and anti-inflammatory effects. However, cysLT (products of 5-LOX enzyme) receptor antagonists selectively repress inflammation.

Both drugs have different mechanisms of anti-inflammatory action and, therefore, can provide simultaneous and/or synergistic potential. Furthermore, both CX and MKT, being highly lipophilic compounds, exhibit low oral bioavailability (60 % for celecoxib and 64 % for montelukast) after oral administration owing to their poor aqueous solubility profiles (1.15 μg/mL for CX, 0.2-0.5 μg/mL for MKT). Improving solubility and dispersion can enhance their bioavailability, decrease dose and limit side

effects. Moreover, presence of common functional groups e.g. amine and carbonyl groups in their structure require similar conditions for their co-conjugation onto AgNPs [11, 66, 67].

Therefore, the selected drugs were co-adsorbed onto the synthesized silver nanoparticles that were then surface modified by PVA coating. Surface coating with hydrophilic polymer and nano-sizing were employed to enhance solubility and reduce the effective concentrations, thereby, possibly further reducing the side effects associated with the active drugs. Also, the particle size of AgNPs was controlled and modified through drug conjugation as well as polymer coating to avoid size-related toxicity risk. The developed, multipurpose, formulation was then characterized from physical and chemical viewpoints and was evaluated for its anti-inflammatory and anti-neoplastic potentials.

2. **Materials and Methods**

2.1 Synthesis of bare silver nanoparticles (AgNPs)

Turkevich method [68] was employed to synthesize silver nanoparticles (AgNPs). In brief, 1 mM silver nitrate ($AgNO_3$) and 40 mM sodium borohydride ($NaBH_4$) solutions were prepared in deionized water. $NaBH_4$ was prepared with ice chilled water and then added drop wise to 1 mM $AgNO_3$ solution kept under gentle stirring. The mixing ratio in volume was 10**:**1 for $AgNO_3$ and $NaBH_4$ respectively. The mixture was kept under gentle stirring for 4 h and meanwhile observed for color changes as an indication of AgNPs synthesis. In consideration of AgNPs separation, the mixture was centrifuged for 4 h at 13500 rpm keeping temperature below 10 °C (Hermle labortechnik, Z-206A, Germany). Resulting pellet of AgNPs was collected by discarding the supernatant. Pellet was then dried through freeze drying [69, 70].

2.2 Synthesis and purification of drugs conjugated AgNPs (NF)

Turkevich method [68] was used with some modifications to synthesize drugs conjugated silver nanoparticles (Figure 1). 1 mM solutions of celecoxib (CX) and montelukast (MKT) were prepared in

ethanol. 1 mM $AgNO_3$ and ice chilled 40 mM $NaBH_4$ solutions were also produced in deionized water. In consideration of determining optimum concentrations of CX, MKT and $AgNO_3$, different ratios were tested. These ratios in volume varied from 1:1:1 to 6:1:1 ($AgNO_3$: CX : MKT). However, $AgNO_3$: $NaBH_4$ in volume was always 10 : 1. CX and MKT solutions were slowly added to $AgNO_3$ solution while maintaining continuous stirring. Resulting mixture was stirred for 30 minutes and color changes were observed. $NaBH_4$ solution was then added drop wise to the mixture under gentle stirring. This mixture was closely observed for any color change and then put through stirring for next 4 h. Conjugation of CX and MKT with AgNPs was indicated by color changes [69, 70].

In order to purify the developed nanoparticles, the eventual mixture was then centrifuged at 13500 rpm at 10 °C for 5 h. Resulting pellet containing the nanoparticles, was collected by discarding the supernatant. Pellet was then subjected to freeze drying. CX and MKT conjugated AgNPs were coded as 'Nanoformulation' or 'NF'.

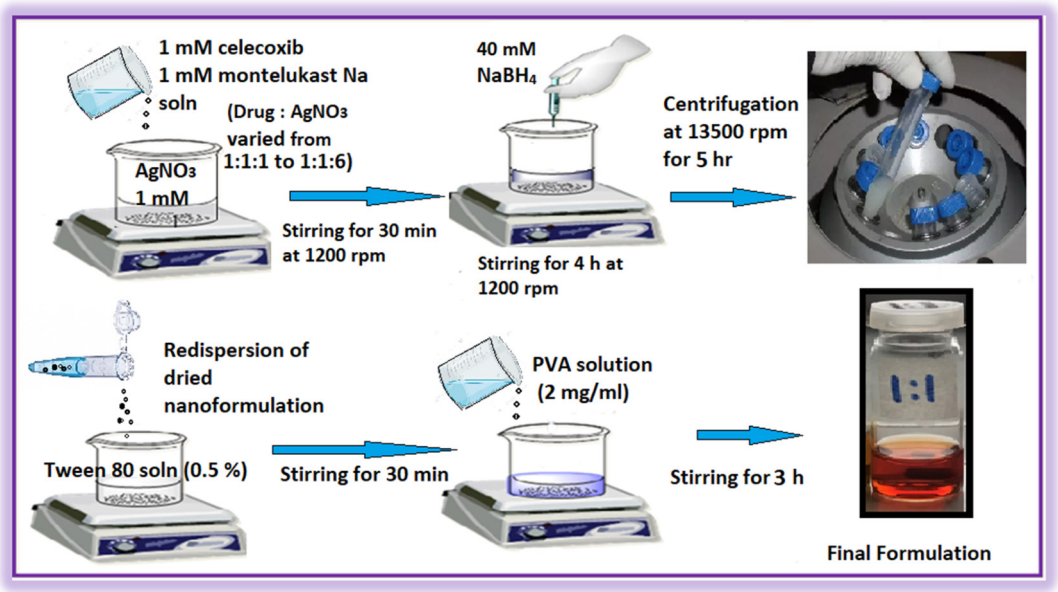

Figure 1 Flow chart representing the procedure of nanoformulation synthesis.

2.3 Synthesis and purification of polymer-coated Nanoformulation (NFC)

0.5 % Tween 80 solution in ethanol and PVA solution (2 mg/mL) in deionized water were prepared. 10 mg purified CX and MKT conjugated AgNPs (NF) were dispersed in 5 mL Tween 80 solution. After stirring for 30 minutes the mixture was poured drop wise into 5 mL of PVA solution (Figure 1). Final mixture was kept under continuous stirring for next 3 h and then subjected to centrifugation at 13500 rpm at 10 ºC for 1 h. Pellet was collected and then freeze dried. PVA coated NF (CX and MKT conjugated AgNPs) was labeled as 'Coated Nanoformulation' or 'NFC'.

Further research including characterizations, *in-vitro* and *in-vivo* studies, was accomplished by separately dispersing silver nanoparticles (AgNPs), nanoformulation (NF) and coated nanoformulation (NFC) into adequate amounts of deionized water.

2.4 Physical and thermal characterizations

Developed nanocarriers were characterized through fundamental and diverse characterization techniques. UV/Visible spectrophotometer (Perkin Elmer, Lambda 25) was used to register absorption/optical spectrum. JASCO, FTIR 6600 spectrometer was employed to inscribe vibrational characteristic spectra of test samples. Scanning range was set from 400-4000 cm^{-1} at 2 mm/s with 4 cm^{-1} resolution and 45° incident angle. FTIR analysis was performed at ATR mode using solid samples. The XRD patterns and crystallographic structures of nanomaterials were documented (on scanning mode) using X-Ray diffractometer, with LYNEX EYE detector (D8 ADVANCE, BRUKER) at 1.2°/min employing (Cu Kα) radiations (λ=1.54 Å, generator voltage = 40 kV, current 40 mA, angular range of 2θ =10°–80°). Zeta potential, mean diameter and polydispersity index (PDI) of the test samples were assessed through dynamic light scattering (DLS) utilizing Zetasizer (Nano ZS-90, Malvern Instruments; Worcestershire, UK). The instrument was equipped with He-Ne laser (λ=635 nm), software version 6.34 along with static scattering angle (90°). 1 mg of test sample in absolute ethanol was sonicated for 40 min. 10 µL of this

transparent solution was then mixed with 1 mL of deionized water followed by vortexing for 5 minutes. Samples were then analyzed with zetasizer. Results were recorded in triplicate. STA (simultaneous thermal analyzer) was employed to perform TGA (thermogravimetric analysis) and DSC (differential scanning calorimetry) analyses, concurrently. Temperature range was set between 50°C and 800°C with heating rate of 10°C/min in N_2 environment with N_2 flow rate of 30 mL/min. DSC was performed to measure the thermal stability and thermal transition behavior of NF and NFC. Temperature range of 50 - 800°C with heating rate of 10°C/min in N_2 environment with flow rate of 30 mL/min. TGA analysis was conducted to ascertain the thermal behavior as well as weight loss from NF and NFC.

2.5 Elemental analysis by LIBS (Laser Induced Breakdown Spectroscopy)

LIBS is a sturdy, fast and simple technique efficiently employed for the elemental analysis not needing complicated sample preparation. It is currently being employed for examining elemental compositions of a variety of solid, liquid or gaseous materials [71, 72].

In this type of spectroscopy, a laser beam is directed on the sample to generate the plasma state. This plasma cools off after expansion. Meanwhile, excited electrons undergo transitions from higher and excited states to the lower ground states. These electronic transitions or plasma emissions are inscribed through spectrometers. Elemental analysis of drugs conjugated silver nanoparticles (NFC) was performed by using such a technique. Specifications include laser beam at λ=532 nm, 300 mJ pulse duration=6 ns and repetition rate=10 Hz [73, 74].

2.6 Drug loading efficiency (LE) and drug loading capacity (LC)

1 mM solutions of CX and MKT were analyzed through UV-Vis spectroscopy at 254 and 238 nm wavelengths. Drug solutions were then poured slowly in to 1 mM $AgNO_3$ solution in 1:1:1 (ratios in volume) maintaining continuous stirring. 40 mM $NaBH_4$ solution was mixed dropwise in to the mixture to develop NF. The final mix was centrifuged (13500 rpm, 4 h) and supernatant was analyzed at 215 and 238 nm wavelengths for the quantitative analysis of celecoxib and montelukast, respectively. The

following equations were used to calculate loading efficiency and loading capacity [63, 65, 69, 70, 75, 76],

$$Loading\ Capacity\ (\%) = \frac{Drug\ (Total) - Drug\ (supernatant)}{Nanoparticles\ (Total\ amount)} \times 100 \qquad (1)$$

$$Loading\ Efficiency\ (\%) = \frac{Drug\ (Total) - Drug\ (supernatant)}{Drug\ (Total)} \times 100 \qquad (2)$$

2.7 *In-vitro* drug release

Drug release mechanism was observed in 4 different physiological environments including pH 7.4, 6.8, 4.5 and 1.2 maintaining temperature at 37 °C ± 0.5 °C. These conditions were maintained with the help of acetate buffer and phosphate buffer saline (PBS) media. Drug release pattern was also determined by applying several mathematical drug release kinetic models such as Korsmeyer-Peppas, Higuchi, 1st order and zero order release kinetics; the relevant. R^2 values were calculated a well. Briefly, specific amounts of NFC were dispersed separately in dialysis bags, previously filled with release media. The bags composed of dialysis membrane with MWCO = 1 kDa and 11.5 mm diameter (CelluSep®) were then submerged into different physiologic release media under gentle stirring (100 rpm). Samples were drawn after predetermined intervals and sink conditions were maintained. Concentrations of CX, MKT and AgNPs were evaluated in triplicate through spectroscopy at their characteristic maximum absorbance wavelengths. Following formula was applied to ascertain the percent drug release [77],

$$Drug\ release\ in\ percent = \frac{Drug\ released\ at\ time\ (t)}{Total\ drug\ loaded} \times 100 \qquad (3)$$

2.8 Protein denaturation (*in-vitro* anti-inflammatory) assay

Inflammation inhibition potential was reveled via *in-vitro* protein denaturation assay. Anti-denaturation activity against bovine serum albumin (BSA) was evaluated. Test, standard and control samples were prepared, incubated (37 °C, 20 min) and heated moderately (55 °C) for only 5 min. Absorbance was recorded afterwards through a UV-Spectrophotometer at 660 and 280 nm wavelengths. Samples, as

required, were diluted before spectroscopy via phosphate buffer of 6.3 pH. Control represented absolute protein (BSA) denaturation.

Standard mixtures were prepared by mixing 0.5 % w/v BSA solution with diclofenac sodium solutions of different concentrations at 9**:**1 v/v respectively. Control mixtures were prepared by mixing 0.5 % w/v BSA solution with deionized water at 9**:**1 v/v respectively. Test mixtures were prepared by mixing 0.5 % w/v BSA solution with test solutions at 9**:**1 v/v respectively.

Percent denaturation inhibition of BSA protein was determined using the given formula [78-83],

$$Percent\ denaturation\ inhibition\ = \frac{Absorbance\ (control) - Absorbance\ (sample)}{Absorbance\ (control)} \times 100 \quad (4)$$

2.9 Cell studies

2.9.1 Cell Culture

Cancer and normal cell lines were obtained from ATCC and cultured in conformity to product guidelines. Briefly, MCF-7 (human breast cancer), Hep-G2 (human Caucasian hepatocyte carcinoma) cells and THLE-2 (human primary hepatocytes) were cultured in DMEM at 37 °C and 5 % CO_2. The growth medium was supplemented with penicillin (50 IU/mL), streptomycin (50 IU/mL) and FBS (10 %), Gibco™, Thermo Fisher Scientific) inactivated with heat, achieving 70-80 % near confluence.

2.9.2 Cytotoxicity assay

3-(4,5-dimethylthiazol-2yl)-2,5-diphenyl-tetrazolium bromide (MTT)-based assay was performed to evaluate cytotoxic potential against human breast adenocarcinoma (MCF-7) cell line, human Caucasian hepatocyte carcinoma cells (Hep-G2) and THLE-2 (human primary hepatocytes). Cancer cells were seeded and grown (96-well plate) in growth medium (100 µL). The cells were added in wells in specified concentrations (1×10^4 cancer cells/well). Specified wells were treated with gradually rising concentrations (5, 7.5, 10, 20, 30 and 40 µg/mL) of AgNPs, NF, NFC, CX and MKT. Cells were then

treated with MTT and incubated for 5 h with 5 % CO_2 supply at 37° C. Incubation was followed by DMSO treatment to dissolve the colored (purple) formazan crystals. Afterwards, absorbance of each well was recorded at 570 nm and 690 nm, and optical densities were determined (Multimode Microplate Reader Instrument, FLUOStar®Omega). The following formula was applied to calculate percent cell viability and half maximal lethal concentration was then determined from these data [43, 77, 84-86].

$$Cell\ viability\ in\ percent = \frac{OD\ (Treated\ samples)}{OD\ (Control\ samples)} \times 100 \qquad (5)$$

2.9.3 Hemo-compatibility evaluation

5 ml samples of blood were collected from healthy human volunteers. The procedure has been demonstrated in Figure 2. Blood samples were collected in heparin coated vacutainer tubes and diluted with PBS (phosphate buffered saline) in 9 (PBS) **:** 1 (blood) v/v [87-89]. 1 mL from this diluted blood was mixed separately with 100 µL of AgNPs (Test), NFC (Test), PBS (as negative control) and 0.1 percent Triton X-100 (as Positive control). Resulting mixtures were then incubated for next 24 h at 37 °C and then centrifuged at 4 °C and speed of 13500 rpm for 10 min. Afterwards, supernatants were examined for their absorbance at 540 nm wavelength using micro-titter plates reader. Extent of hemolysis was computed by applying the following formula [22, 23],

$$Hemolysis\ in\ percent\ = \frac{Test\ (540) - Negative\ control\ (540)}{Poaitive\ control\ (540) - Negative\ control\ (540)} \times 100 \qquad (6)$$

where, the values in the formula correspond to optical densities of test samples, positive and negative control.

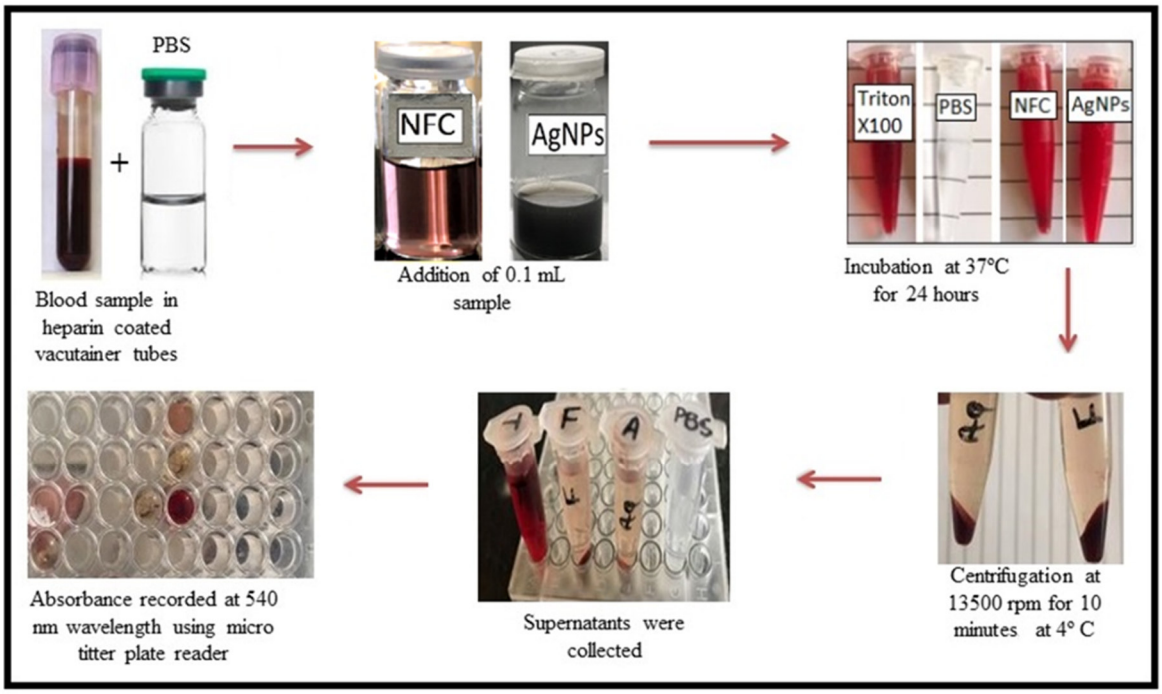

Figure 2 Flow chart representing the procedure of hemo-compatibility assay.

2.10 *In-vivo* studies

2.10.1 Animals and Animal Models

Animal studies were carried out under the prior approval from Bio-Ethical Committee (Protocol #BEC-FBS-QAU2020-214) of Quaid-i-Azam University, Islamabad, Pakistan. Healthy albino mice (weight = 20-30 g and age = 4-5 weeks) and albino rats that (300-500 g) were obtained from NIH (National Institute of Health), Islamabad, Pakistan. Standard conditions were well maintained which included pathogen-free environment, humidity level of 55 ± 5 %, light/dark cycle of 12 h and moderate temperature (22 ± 1 °C). Mice were supplied with water ad libitum, fed with standard food and were used only in this single study. Guidelines were followed for the care and use of mice as experimental laboratory animals. Mice were

arranged in groups. Oral dose administration was performed through gastric gavage. Animal groups and respective details are shown in Table 1.

Table 1. Animal groups and associated details for *in-vivo* activity.

Group classification	**Group**	**Administered substance**	**Dose**
Standard	A.	Celecoxib	25 mg/kg
	B.	Montelukast sodium	20 mg/kg
Control	Positive	Normal saline	
	Negative	Brewer's yeast or Carrageenan only	
Treatment	i.	NF	0.5 mg/kg
	ii.	NF	1 mg/kg
	iii.	NF	2 mg/kg
	iv.	NFC	0.5 mg/kg
	v.	NFC	1 mg/kg
	vi.	NFC	2 mg/kg
	vii.	AgNPs	0.5 mg/kg
	viii.	AgNPs	1 mg/kg
	ix.	AgNPs	2 mg/kg
	x.	Physical mixture of CX, MKT, AgNPs and PVA	2 mg/kg

2.10.2 Anti-inflammatory assay (carrageenan induced inflammation model)

Carrageenan induced inflammatory (i.e. paw edema) model was employed to evaluate anti-inflammatory potential. Animals were treated with predetermined oral doses of test formulations and standard. After 1 h, 0.2 mL of 0.1 % carrageenan solution was administered in to one hind paw of each mouse. Paw volumes were assessed at specified time intervals before and after carrageenan injections using dial thickness gauge meter instrument, (Model No. F 2046, Mitutoyo Kawasaki, Japan). Percent inhibition of inflammation was calculated as per the given formula [64, 90-92],

$$Inflammation\ Inhibition\ (\%) = \frac{V_{control(negative)} - V_{Test\ sample}}{V_{control(negative)}} \times 100 \qquad (7)$$

2.10.3 Hot plate thermal hyperalgesia assay (carrageenan induced inflammation model)

The 'hot plate thermal hyperalgesia assay' according to Eddy and Leimbach was employed to evaluate thermal hyperalgesia [93]. Animals were treated with predetermined oral doses of test formulations and standard. After 1 h, mice were administered with specified dose of carrageenan. Hot plate temperature was adjusted at 55 ± 2 °C. Mice were placed on hot plate. Paw withdrawal latency (i.e. the time that evokes paw licking, withdrawal and jumping responses) was observed with a cut-off time of max 30 s. The values were noted at 0, 2, 4 and 6 h time intervals following carrageenan treatment [64, 65, 94].

2.10.4 Antipyretic activity evaluation in mice model (brewer's yeast induced pyrexia model)

Both male and female mice were involved in the study. Animals were fasted for 12 h providing only water ad libitum. Rectal digital thermometer was used to determine baseline body temperature. Pyrexia induction was achieved through subcutaneous injection of brewer's yeast (20 %). Body temperature was again determined after 18 h of the injection. Selected mice (showing temperature rise of > 0.5 °C) were

administered with oral doses of test formulations and standard. Afterwards body temperatures were determined at specified 0, 1, 2 and 3 h time intervals [95, 96].

2.10.5 In-vivo anti-cancer activity evaluation in xenograft mice models

Anti-tumor activity was evaluated in orthotopic breast cancer and subcutaneous liver cancer xenograft mice models. Human breast cancer MCF-7 and liver cancer Hep-G2 cell lines were established and grown as per the protocol explained earlier.

Orthotopic breast cancer establishment

Female albino mice were separated for the studies. Skin areas near nipple 2 and 3 were shaved and cleaned with 70 % ethanol. Tumor cell suspension (2×10^6 cells in 0.1 ml PBS) was resuspended and then injected into 2^{nd} or 3^{rd} mammary fat pads [97, 98].

Subcutaneous liver cancer establishment

Mixed female and male albino mice were selected. Skin areas near flank regions were shaved and cleaned with 70 % ethanol. Tumor cell suspension (2×10^6 cells in 0.1 ml PBS) was resuspended and then injected subcutaneously into flank regions of mice [97, 99].

Three days after tumor inoculation, mice were organized into the following 03 groups with 6 mice each, along with the 4th group that served as positive control. Mice in this group were normal mice without cancer cell inoculation. Group summary and post-injection treatments were as follows:

Standard group: Tamoxifen 10 mg/kg/oral/OD (once daily) for 14 days (for orthotopic breast cancer model) and 5-fluorouracil (5-FU) 25 mg/kg/oral daily for 14 days (for subcutaneous liver cancer model).

Treatment group: NFC 10 mg/kg/oral/OD for 14 days.

Negative Control group: Normal saline oral/OD for 14 days.

Positive Control group: Normal saline oral/OD for 14 days.

Tumors were monitored and evaluated after every 3 days with a Vernier caliper. Mice were euthanized on the 18th day of tumor inoculation; tumors were excised and weighed. Tumor volumes were evaluated employing the following formula [97-101],

$$Volume\ of\ excised\ tumor = Length\ of\ tumor \times (width\ of\ tumor)^2 \times 0.5 \quad (8)$$

Percent tumor inhibition was also calculated as follows [98],

$$Tumor\ Inhibition\ (\%) = \frac{A - B}{A} \times 100 \quad (9)$$

where,

A = average weight of tumor mass in Negative control group,

B = average weight of tumor mass in Treatment/Standard group.

2.10.6 Bioavailability studies

The research was done in accordance with the 1986 Animals Act, U.K. keeping with the guidelines of EU Directive for animal studies (2010/63/EU). All the animal experiments were carried out in conformity with the guidelines from National Institute of Health (NIH Publication No. 8023, revised 1978) for the care and use of experimental laboratory animals. The bioavailability study was performed with 36 albino rats that were healthy and weighed almost 300-500 g. Rats were organized in to 3 different groups, each group of which included 12 animals. Albino rats were fed with standard diet. Group A received specified oral doses of celecoxib. Similarly, each animal in group B received montelukast, while animals in group C received oral doses of NFC. Animals were then subjected to blood sample collection from femoral artery (right). Twelve blood samples were drawn from a single group at predetermined intervals of time. Each animal was used only once for blood sampling. Plasma was collected through centrifugation (10,000 rpm, 10 minutes) and analyzed through HPLC technique. For montelukast, bioavailability was determined using 4.6 mm × 5 cm, C-8 column maintaining a constant flow rate (0.9 mL/min), 10 µL sample injection

volume and 280 nm as λ_{max} with tailing factor < 2. Mobile phase used was acetonitrile/methanol mixture in 40:60 ratio (v/v). An equal mixture of acetonitrile and methanol was used as a diluent. [102]. For celecoxib, bioavailability was determined using 4.6 mm × 5 cm, C-18 column maintaining a constant flow rate (1 mL/min), 20 µL sample injection volume and 240 nm as λ_{max}. Mobile phase used was 10 mM phosphate buffer (pH 6.0)/acetonitrile mixture in 54:46 ratio (v/v) [103]. Plasma drug concentrations at different time intervals were evaluated and this plasma data was employed to determine half-life, elimination rate constant, C_{max}, T_{max}, and $AUC_{0\text{-}24h}$ with Kinetica software (Version 4.4).

2.10.7 Acute toxicity study

Mice were organized into treatment and control groups. A single group comprised 5 mice. Specified groups were treated with predetermined increasing doses (25, 50, 65 and 80 mg/kg). Animals were observed for the next 2 weeks as regards for the food consumption, functional observations, behavior, body weight and deaths. LD_{50} was determined from the mortality rate per group [63, 104, 105].

2.11 Statistical analysis

Results are expressed as mean ± SD. All the experiments were conducted in triplicate and outcomes are displayed accordingly. Mean values of obtained results were compared and analyzed by employing one-way analysis of variance (ANOVA), Student's *t*-test followed by Tuckey post-hoc test. Analysis was performed while considering $P < 0.05$ (i.e., 0.05 was the significance level).

3. Results and Discussion

3.1 UV-Visible spectroscopy

Color changes of the final mixtures indicated the synthesis of bare silver nanoparticles and drugs conjugated silver nanoparticles, designated as AgNPs and Nanoformulation (NF), respectively. AgNPs showed greyish brown color, while that of different NFs ranged from wine red (barn red) to black.

Successful synthesis of AgNPs and NFs was further confirmed through SPR peak analysis. AgNPs and different NFs display surface plasmon resonance (SPR) absorbance peaks at 392 nm and in the range of 402-446 nm, respectively (Figure 3). NFs manifest additional absorbance peaks in the range of 230-260 nm corresponding to λ_{max} of montelukast (238 nm) and celecoxib (254 nm) [60, 106, 107]. Red shifts in SPR absorbance peaks of NFs are attributed to the conjugation of drugs on AgNPs. NF with 1:1:1 ratio ($AgNO_3$: CX : MKT) was selected as the optimized one for further studies due to its preferable and superior properties including high reproducibility, brighter color and sharp absorbance peak at 422 nm.

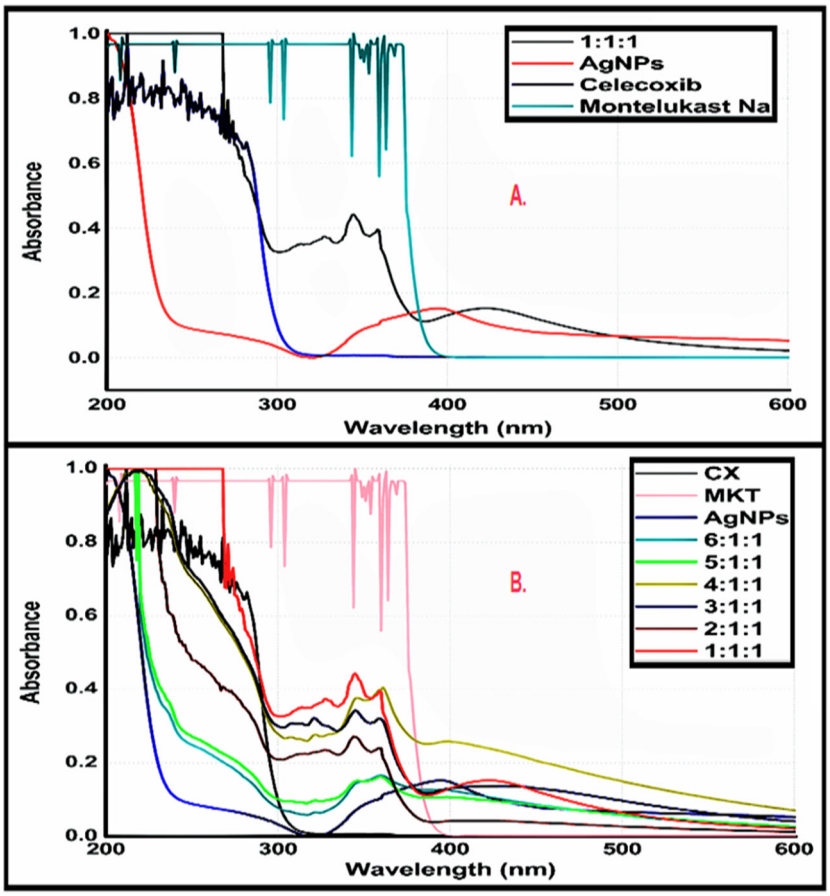

Figure 3 Results of surface plasmon resonance analysis. **A)** Selected results only **B)** Detailed comparison. Ratios correspond to $AgNO_3$: CX : MKT, respectively.

3.2 Powder X-Ray diffraction (PXRD) analysis

XRD patterns of PVA, celecoxib, montelukast, AgNPs, NFC, and NF are shown in Figure 4A. AgNPs exhibited characteristic peaks at 2θ values of 38.11°, 44.27° and 64.42°. These peaks correspond to (111), (200) and (220) planes confirming the crystalline 'cubic' structure of the nanoparticles [50]. The XRD spectrum of celecoxib revealed a crystalline nature as well with sharp diffraction peaks at 2θ values of 5.3°, 10.8°, 16.1° and 21.6° [108, 109]. PVA exhibited partially amorphous nature with a peak around 15° while montelukast exhibited amorphous nature with no distinct peak [67, 108, 110]. The XRD spectrum of NF showed small peaks (around 38° and 64°) with very low intensities corresponding to (111) and (220) planes of AgNPs. Reduced intensities indicated the conversion of crystalline AgNPs into partially amorphous form. Moreover, absence of any other distinctive peak confirms the conversion of crystalline celecoxib into amorphous form. Whereas, the XRD patterns of NFC revealed peaks of AgNPs and PVA around 38° and 15°, respectively. However, these peaks show very much reduced intensity and depict the efficient PVA coating over drug conjugated AgNPs. No other distinctive diffraction peak in XRD pattern of NFC suggests the conversion of crystalline celecoxib and AgNPs into amorphous and partially amorphous forms, respectively. The final formulation (PVA coated drug conjugated AgNPs) exhibited overall amorphous nature with no sharp intense peaks, which is associated with greater solubility and, hence, better dispersion properties.

3.3 Fourier transform infrared spectroscopy (FTIR) analysis

The comparative IR spectra of NFC, NF, PVA, AgNPs, celecoxib and montelukast are displayed in Figure 4B. AgNPs, being metallic substances, did not produce any characteristic mark in finger print or functional group regions. FTIR spectrum of celecoxib showed its characteristic peaks at 3336 and 3224 cm^{-1} (primary/secondary amines), 3087 cm^{-1} (aromatic CH_2 stretching), 1594 and 1560 cm^{-1} (amine bending), 1450 cm^{-1} (aromatic C=C), 1346 and 1131 cm^{-1} (asymmetric/symmetric stretching of S=O in SO_2), 1226 and 1070 cm^{-1} (CF_3) [66, 86, 109, 111, 112]. Montelukast displayed the bond vibrations at

3380 cm^{-1} (COOH stretching), 3087 cm^{-1} (aromatic C − H stretching), 2930 cm^{-1} (aliphatic C − H stretching), 1582 cm^{-1} (C=O acid's stretching), 1138 cm^{-1} (ether C − O linkage of tertiary alcohol) and 1090 cm^{-1} (C − Cl) [113, 114]. When AgNPs are loaded with celecoxib and montelukast then these drugs are entrapped onto nanoparticles due to the chelation of their amines and carbonyl groups (chelating agents) to the surface of AgNPs (electron deficient center). Therefore, the characteristic stretching vibrations of amines and C=O did not appear in NF spectrum [115]. The peak positions of other functional groups i.e. C−H stretching (aromatic), C−H stretching (aliphatic), aromatic C=C, S=O, C−F, ether C−O linkage, C−Cl were shifted slightly and appeared at 3038 cm^{-1}, 2926 cm^{-1}, 1448 cm^{-1}, 1135 cm^{-1}, 1224 cm^{-1} as well as 990 cm^{-1}, 1168 cm^{-1} and 1023 cm^{-1}, respectively. NFC spectrum suggested the successful capping of NF with PVA and Tween 80. Broad band from 3100-3500 cm^{-1} in NFC spectrum represents the OH groups in PVA and Tween 80 [112, 116]. Peaks appearing at 2926 and 2859 cm^{-1} correspond to −CH stretchings in PVA and Tween 80. Vibrational peak at 1739 cm^{-1} represents the carbonyl stretching due to ester group in Tween 80 [115, 116]. Furthermore, peaks at 1459 cm^{-1}, 1347 cm^{-1}, 1247 cm^{-1}, 1146 cm^{-1}, 1090 cm^{-1}, 955 cm^{-1} correspond to aromatic C=C, asymmetric stretching of S=O, C−F, symmetric stretching of S=O, C−O and C−F groups in drugs, respectively. These FTIR spectra suggested successful conjugation of drugs on AgNPs in 'NF' and efficient PVA capping in 'NFC'.

3.4 Average diameter, PDI (polydispersity index) and Zeta potential determination

Results are shown in Figure 5. Biological effects of silver nanoparticles is associated with their particle size. In virtue of their enhanced total surface area, wide distribution and improved penetration in multiple organs, AgNPs with shorter size range (< 100 nm) elicit pronounced acute toxicity [49, 50, 117, 118]. Conjugation of drug molecules on AgNPs increased the particle size ten times, from ~20 nm to ~204 nm. PVA coating further modified the particle size to 304 nm possibly repressing the size-dependent toxicity associated to AgNPs. However, such particles showed very low zeta potential of -1.6 mV. Surface modification with PVA provides stability by imparting slight negative surface charge (-14 mV) and

avoiding aggregation. Moreover, slight negative surface charge along with nanometric dimensions (10-500 nm) is preferred for efficient cellular uptake [49, 52, 55].

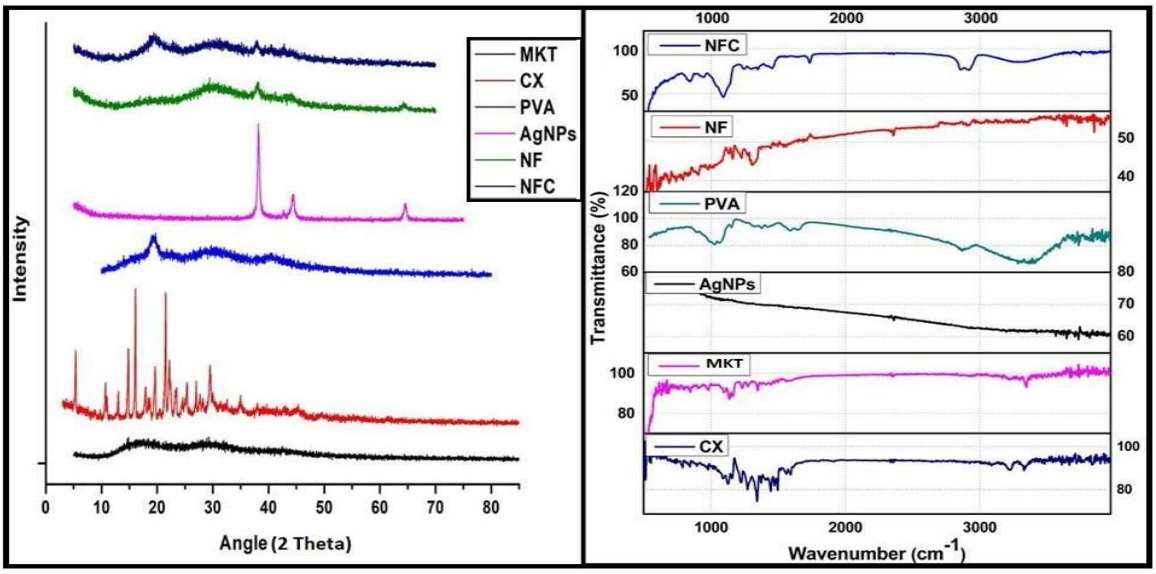

Figure 4 Results of A) PXRD and B) FTIR analysis.

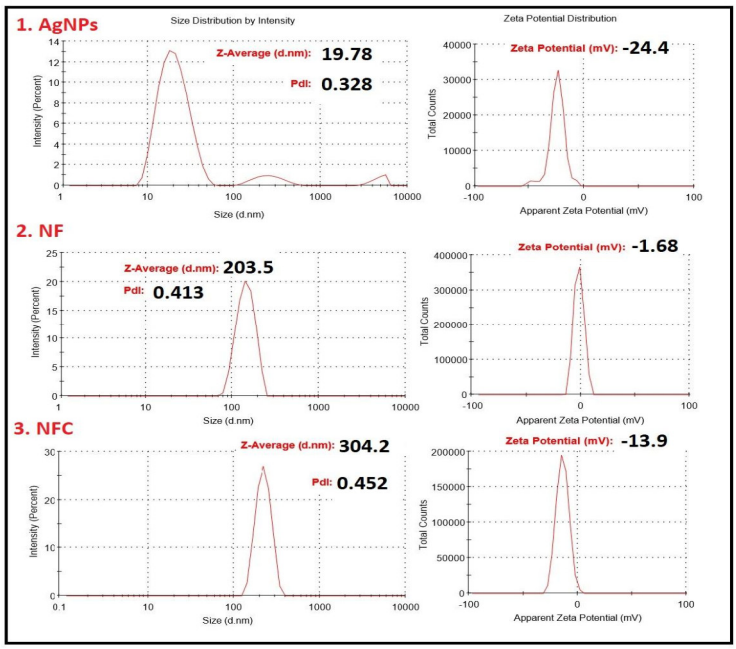

Figure 5 Particle size, zeta potential and PDI of **1)** AgNPs, **2)** NF and **3)** NFC.

3.5. Thermal analyses

3.5.1 Differential scanning calorimetry analysis (DSC)

Thermal behavior was analyzed to further evaluate the crystalline nature of celecoxib, montelukast, PVA, NF and NFC and the results are shown in Figures 6A and 6B (blue lines). Pure celecoxib exhibits sharp endothermic peak around 160 °C, corresponding to the melting point of crystalline CX [59, 108, 119]. DSC curves of montelukast and PVA depict their amorphous natures [67, 74, 108]. Montelukast showed a broad endothermic peak at about 142 °C which might be attributed to its melting point [74]. Thermograms of NF and NFC exhibit broad peaks around 160 °C and 142 °C corresponding to the melting points of celecoxib and montelukast respectively [59, 74, 108, 119, 120]. Absence of sharp peak around 160 °C indicates the conversion of crystalline CX into amorphous form. An endothermic peak around 458 °C in the DSC curve of NF (Figure 6A) can be ascribed to the melting point of metallic Ag (silver) in nanoformulation. This peak was showed a slight shifted towards 470 °C in the DSC curve of NFC. It can be ascribed to surface modification of nanomaterials through PVA coating. Surface coating with this amorphous polymer provided stabilizing effect. Melting point decrement of silver from 961 °C (metallic Ag) to 458 °C (Ag nanoparticles) might possibly be attributed to size reduction due to nano-sizing [121, 122], enhanced surface/volume ratio, conjugation of drugs and characteristic crystalline formations of Ag nanoparticles.

3.5.2 Thermo-gravimetric analysis (TGA)

Results of TGA analysis are shown in Figures 6A and 6B (black lines). These curves suggest that the formulations exhibited loss in their weights at higher as well as lower temperature owing to degradation and water evaporation, respectively. NF showed 24 % weight loss possibly due to the vaporization of adsorbed water (Figure 6A). TGA curve of NFC (Figure 6B) exhibited 43 % weight loss which might be attributed to interlayer as well as surface adsorbed water vaporization and pyrolysis of PVA [123]. The

weight loss due to evaporation of water appeared in the earlier region of curve i.e. from 80 °C to 120 °C. On the contrary, pyrolysis of PVA led to weight loss in the later region of curve from 230 °C to 360 °C [123, 124].

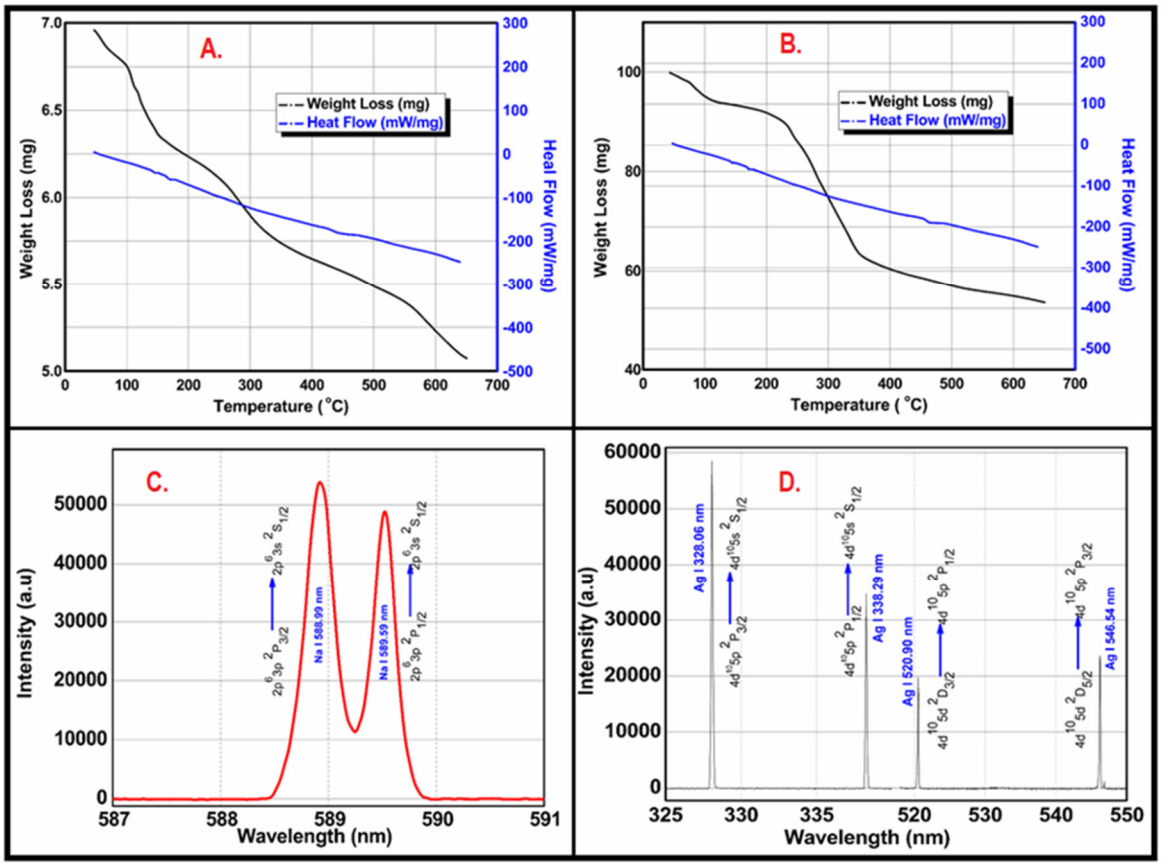

Figure 6 DSC curves (blue lines) of NF (**A**) and NFC (**B**), respectively. TGA curves (black lines), NF in Figure (**A**) and NFC in Figure (**B**). Figures (**C**) and (**D**) show NFC LIBS analysis spectra. The spectroscopic signature of silver (Ag) and sodium (Na) observed in NFC emission spectrum.

3.6 Elemental analysis

Spectrum from the LIBS analysis, exhibited distinct peaks which correspond to neutral silver (from AgNPs) and sodium (from montelukast). These peaks are marked in the LIBS spectra shown in Figures 6C and 6D. The analysis describes the elemental composition of the final formulation (NFC), suggesting the presence of AgNPs and the conjugated drugs, montelukast and celecoxib in the final formulation. Laser induced breakdown spectroscopy further confirms the actual conjugation of drugs on the surface of AgNPs.

3.7 Drug loading efficiency (LE) and drug loading capacity (LC)

Drug loading efficiencies were ascertained to be 31 % and 42 % for montelukast and celecoxib, respectively. Total loading capacity was revealed to be 39 % with individual loading capacities of 22 % and 17 %, respectively.

Outcomes of the release study are shown in Figure 7. The release pattern of NFC was determined and R^2 value was ascribed to 1st order release kinetics (Figure 7A). Conjugated drugs were released from AgNPs in a sustained manner. The pattern was consistent in all the three tested media with the best release observed in 4.5 pH medium. Both the conjugated drugs exhibited distinct release profiles but with the same pattern. Montelukast, after 12 h, showed 64, 68, 95 and 74 % release whereas for celecoxib the values were 62, 79, 90 and 74 % in 7.4, 6.8, 4.5 and 1.2 pH media (Figure 7B). However, both of them manifested maximal release in moderately acidic milieu i.e. 4.5 pH medium as shown in a separate Figure 7C for better understanding. It also unveils the potential for passive tumor targeting as the NFC can release drugs preferably in tumor microenvironment and cells which have moderately acidic conditions.

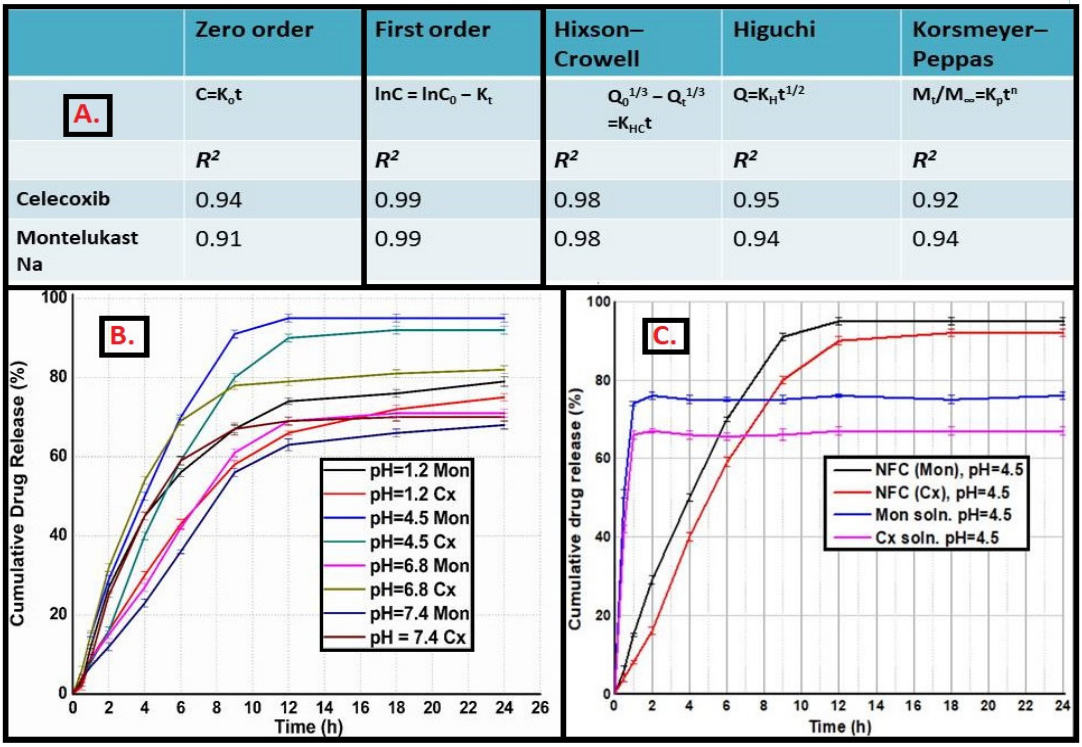

Figure 7 Results of drug release studies: *In-vitro* NFC pharmacokinetic modeling (**A**). *In-vitro* drugs release analysis in three different physiological environments including pH 7.4, 6.8, 4.5 and 1.2 (**B**). Maximal *in-vitro* drug release in (moderately acidic milieu) 4.5 pH medium (**C**).

3.8 Anti-denaturation activity

Inflammation can aggravate cancer as it leads to protein denaturation, halting the essential processes. Therefore, anti-denaturation is an important aspect to be discovered in order to evaluate anti-inflammatory activity. Bovine serum albumin (BSA) exhibits maximum absorbance characteristic peak in the range of 275-280 nm. In order to denature the BSA, it was heated at 55 °C. Vanished maximum absorbance peak further confirmed the denaturation (Figure 8). Different concentrations of standard drugs, blank silver nanoparticles, NF and NFC were employed in BSA solutions, separately, to examine

their percent anti-denaturation activities (supplementary Figure S-1). Different concentrations used were 60, 90, 120, 150,180, 240, 300 and 400 µg/mL. The concentrations producing > 80 % denaturation inhibition were considered effective. BSA denaturation prevention was confirmed through the presence of BSA characteristic absorbance peak. NFC, NF, physical mixture, AgNPs, montelukast and celecoxib were effective at 60, 90, 150, 180, 150 and 400 ug/mL, respectively. Results indicate strong anti-inflammatory activities of NF and NFC as shown in Figure 9A.

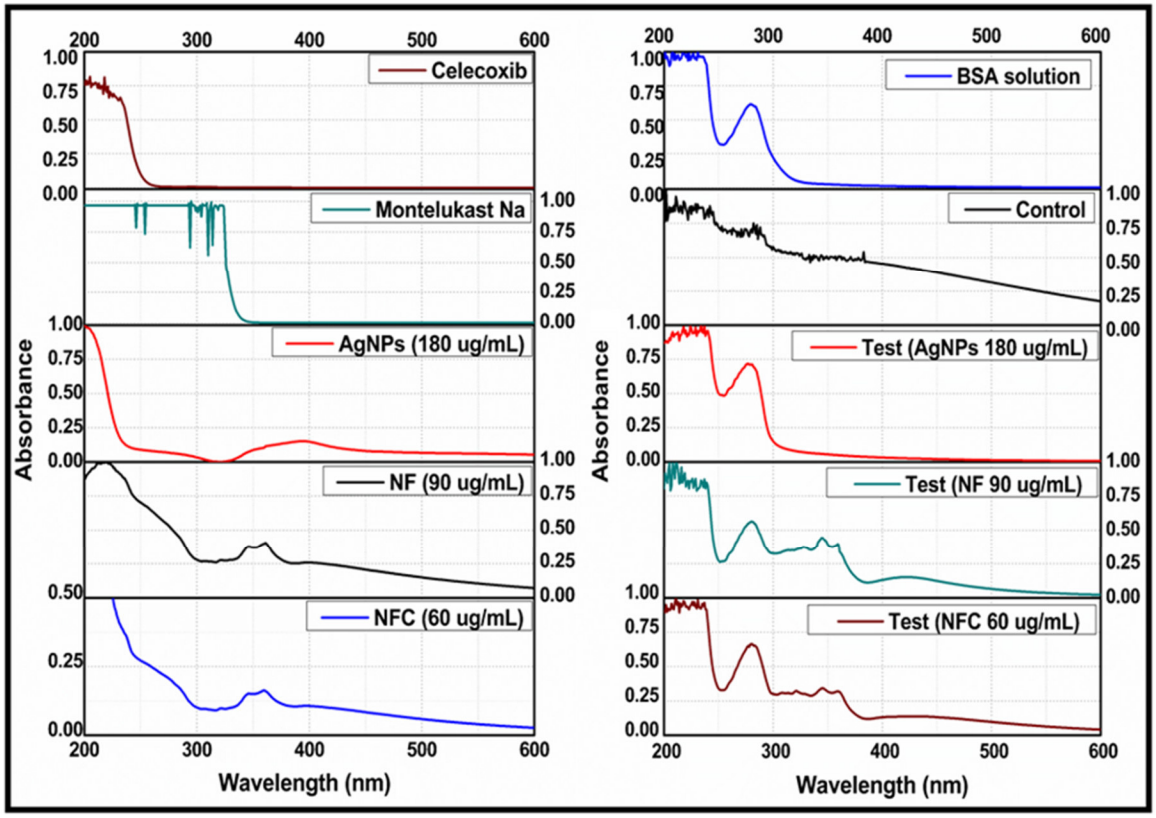

Figure 8 Results of BSA anti-denaturation assay: UV-Absorbance spectra of standard solutions (CX, MKT, AgNPs and BSA solutions), nanoformulations (NF and NFC), control solution and test solutions (minimum w/v concentrations showing anti-denaturation activity).

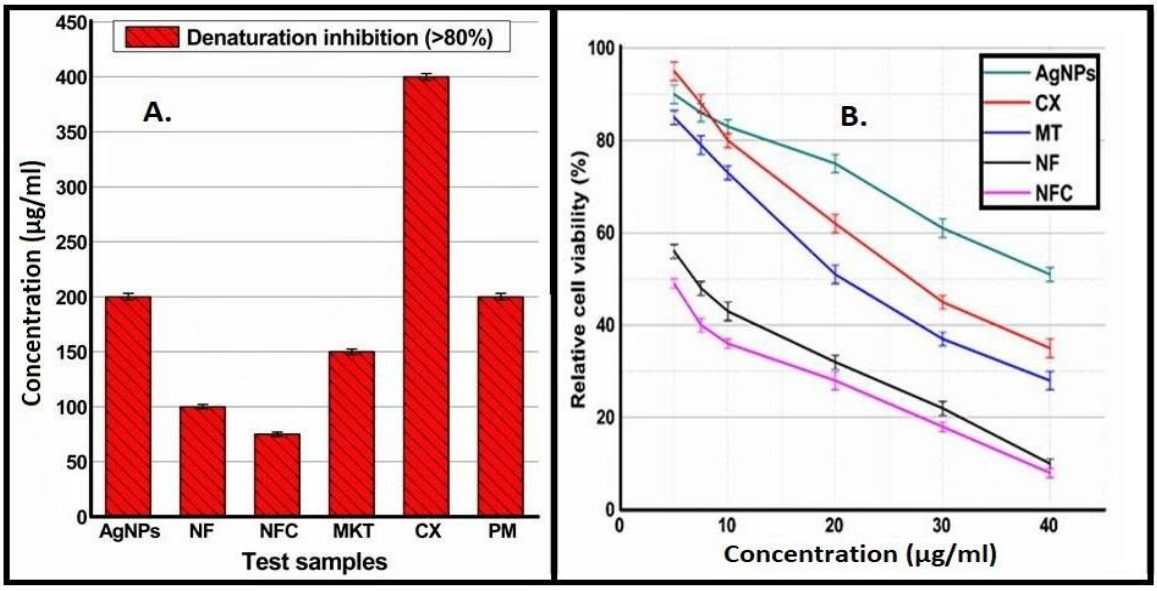

Figure 9 A) Concentrations of physical mixture (PM), celecoxib (CX), montelukast (MKT), NFC, NF and AgNPs producing > 80 % inhibition of BSA denaturation **B)** Percent relative cell viabilities as results of MTT assay against MCF-7 cell line (line graphs).

3.9 Cytotoxicity assay

Results of MTT assay revealed anti-cancer effects of all the tested samples against both MCF-7 and Hep-G2 cancer cell lines. Cytotoxicity of NFC against normal human hepatocytes was found to be negligible.

3.9.1 Anti-cancer activity against MCF-7 cancer cell lines

Nanomaterials showed efficient and dose-dependent anti-cancer effects against human breast adenocarcinoma cells (MCF-7). IC_{50} values for MKT, CX, AgNPs, NF and NFC were found to be 21, 27, 41, 7 and 5 µg/mL, respectively (Figures 9B, 10A). Outcomes suggest the dose-dependent, anti-proliferative activity exhibiting a decreased cell viability and enhanced cytotoxicity with increasing concentrations of examined samples. NF and NFC showed significantly better effects. NFC was the most potent and its better activity as compared to NF might be attributed to its finer dispersion and stability.

IC_{50} values of some standard common anti-cancer drugs in μM concentrations are expressed for comparison in Figure 10B [125-131].

3.9.2 Anti-cancer activity against Hep-G2 cancer cell lines

Nanomaterials expressed potent and dose-dependent anti-proliferative activity against human caucasian hepatocyte carcinoma cells (Hep-G2). IC_{50} values for MKT, CX, AgNPs, NF and NFC were found to be 32, 42, 26, 11 and 7.1 μg/mL, respectively (Figures 11A, 11B). Outcomes suggest the dose-dependent activity exhibiting decreased cell viability with increasing concentrations of examined samples. NF and NFC showed significantly better effects. IC_{50} values of some standard common anti-cancer drugs in μg/mL concentrations are expressed for comparison in Figure 12A [132-137].

Nanomaterials showed strong anti-proliferative activity possibly because of synergistic effects of celecoxib, montelukast and AgNPs, surface modification with biocompatible polymer and nano-sizing. NFC was the most potent against both the cancer cell lines and its better activity as compared to NF might be attributed to its finer dispersion and stability. Cytotoxicity assay revealed the potent anti-cancer activity of synthesized nanoformulation and its potential to become a non-traditional safer and cheaper alternative for more toxic traditional anti-cancer agents.

3.9.3 Cytotoxicity against normal THLE-2 human primary hepatic cells

Cytotoxicity against normal liver cells was determined at the IC_{50} value of NFC against Hep-G2 cancer cells i.e. 7.1 μg/ml. NFC showed negligible cytotoxicity against normal cells at the concentration used. Anti-inflammatory agents show activity against the activated inflammatory pathways. As in normal cells inflammatory pathways are not activated, therefore anti-inflammatory agents showed negligible toxicity.

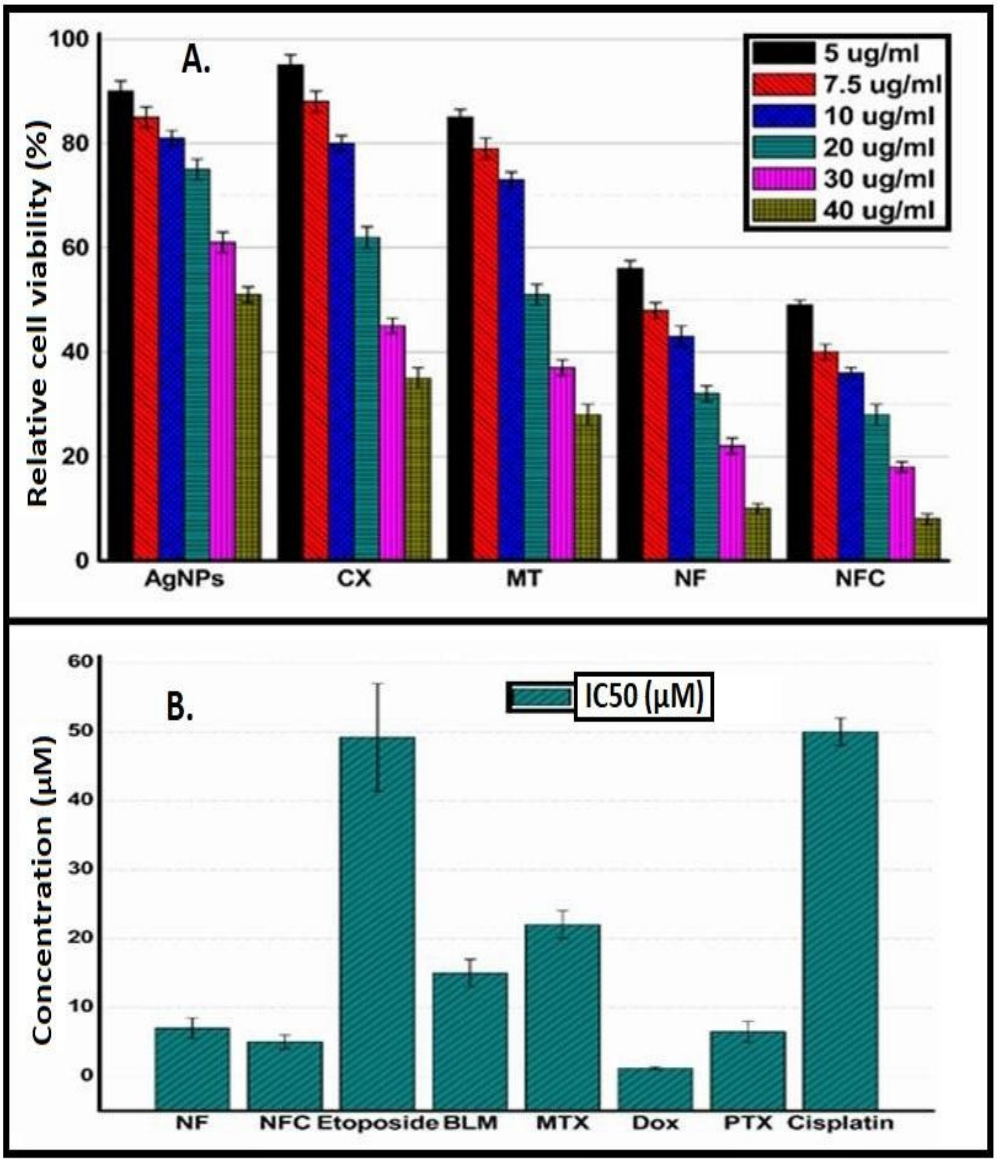

Figure 10 A) Percent relative cell viabilities as results of MTT assay against MCF-7 cell line (bar chart). **B**) Comparison of IC_{50} values of cisplatin (Cis), paclitaxel (PTX), doxorubicin (Dox), methotrexate (MTX), bleomycin (BLM), etoposide (ETP), NFC and NF against MCF-7 cell lines.

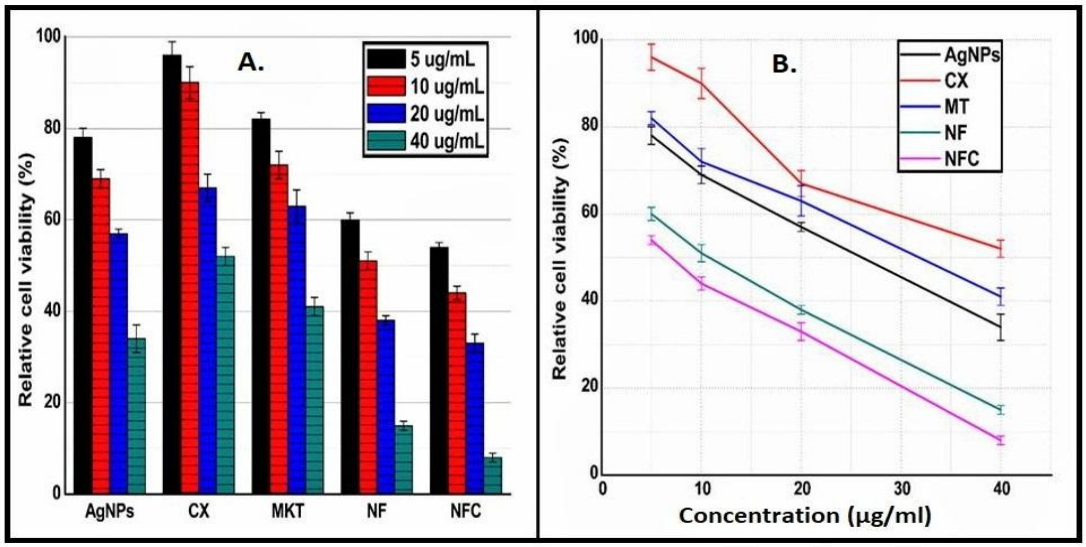

Figure 11 Percent relative cell viabilities as results of MTT assay against Hep-G2 cells. **A**) Bar chart B) Line graphs.

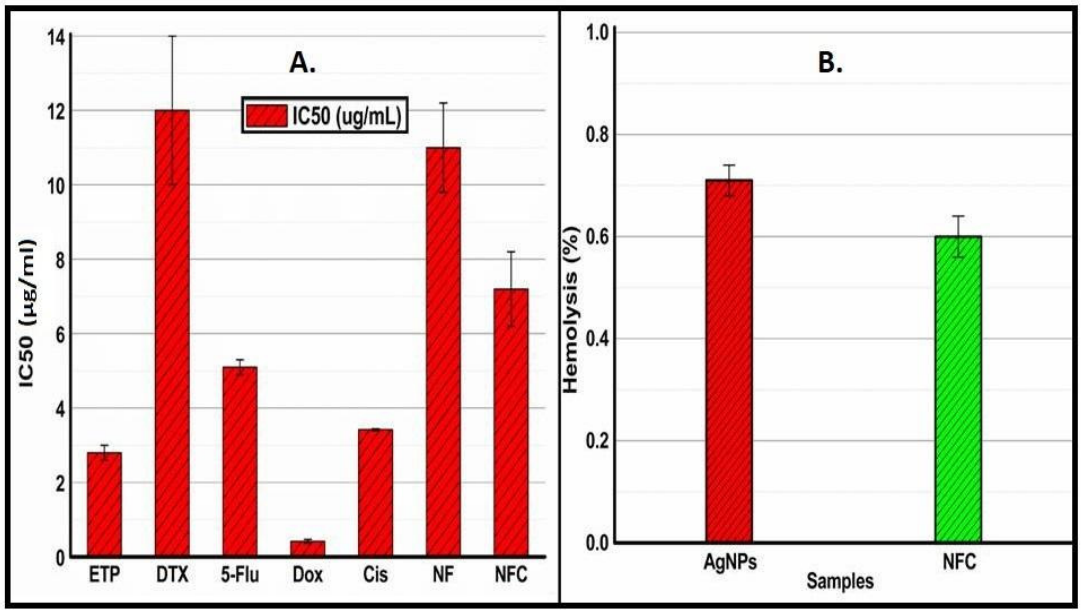

Figure 12 A) Comparison of IC50 values of etoposide (ETP), docetaxel (DCT), doxorubicin (Dox), cisplatin (Cis), NF and NFC against Hep-G2 cell lines. **B)** Percent hemolysis produced by NF and NFC

3.9.4 Hemo-compatibility assay

Hemo-incompatibility leads to lysis of blood cells especially erythrocytes. Therefore, it is an important aspect of the drug formulation and needs to be evaluated. Hemo-incompatibility can cause toxicity through blood complement system and coagulation cascade activation [22]. Human erythrocyte viability was used as an indicator of hemo-compatibility. NFC and AgNPs exhibited 0.60 % and 0.71 % hemolysis, respectively (Figure 12B). The outcomes are well within the acceptable limits, i.e. < 1 % and < 0.8 % as per US FDA and Council of Europe guidelines, respectively [22]. Results indicate hemo-compatible nature of the developed nanoformulation.

3.10 *In-vivo* studies

3.10.1 Effect of nanomaterials on carrageenan induced inflammation (paw edema)

Cancer cells with co-opted and over-expressed inflammatory surface receptors produce signaling molecules including chemokines and cytokines which then potentiate inflammation [9, 10]. Inflammatory factors then lead to neo-angiogenesis, lymph-angiogenesis, tumor growth, immuno-suppression, proliferation and metastasis [11-16]. Therefore, inflammatory cells of tumor niche are critical targets to arrest cancer growth and managing inflammation plays a key role in repressing cancers. Inflammation comprises two phases: in the initial phase serotonin and histamine initiate and extend inflammatory processes, while, the later phase involves prostaglandin synthesis which further propagates the inflammation. This 2nd phase can be ascribed to the activity of cyclooxygenase and lipooxygenase enzymes [138, 139]. Anti-inflammatory activities of NFC, NF, AgNPs, MKT, CX and physical mixture of MKT, CX, AgNPs and PVA are illustrated in Figures 13A, 13B, 14 and supplementary Figures S-2 and S-3**.** It is evident from the graphs that NFC and NF exhibited significantly better effects at 1 mg/kg and 2 mg/kg doses respectively, in comparison to other tested samples as well as the controls. NFC, being the most impressive, showed efficacy at 1 mg/kg dose which was proportional to the activities of MKT and CX at 20 mg/kg and 25 mg/kg doses, respectively. The anti-inflammatory effect of NFC at 2 mg/kg

was remarkably superior than that of the standards at 20 mg/kg (montelukast) and 25 mg/kg (celecoxib) as shown in Figures 13A and 14. Superior action of NFC than NF might be attributed to its greater stability, dispersion, biocompatibility, hydrophilicity, RES avoiding potential and possibly improved cellular uptake due to slight negative surface charge. Further, the modified and sustained release of CX, MKT and AgNPs from overlying PVA coating might possibly be the basis for slightly slow-going actions of NFC in contrast to NF. As, the paw edema inhibition was significant in 4^{th} and 6^{th} hours, the effects of nanofomulations can be ascribed to the 2^{nd} phase of inflammation. Potent anti-inflammatory potential of the synthesized nanoformulation encourages its application in chemotherapy to impede cancer sustaining tumor niche inflammation and recede cancer progression.

Furthermore, the drugs showed 'Sustained release' in all the pH media showing minimum release in the first 2 h as shown in Figure 7. Also, in the bioavailability study T_{max} of drugs were observed to be 6 and 8 h for montelukast and celecoxib, respectively, after oral administration of nanoformulation. Whereas, T_{max} for montelukast and celecoxib solutions were observed to be 1 and 1.2 hours, respectively. This means the drugs were not released in the stomach in the earlier hours after oral administration. Moreover, the anti-inflammatory activity of nanoformulation in paw edema model started showing activity in earlier hours of administration i.e. 1-2 hours and it was almost maximum at 6^{th} h. The activities of drugs in solutions are compared to the nanoformulation in Figure 13. It is shown that nanoformulation showed better activity than drug solutions. As, the drug was not released in the earlier hours of administration in the stomach and nanoformulation showed better activity in *in-vivo* models e.g. paw edema model in the early hours of administration. It implies that the nanoformulation was absorbed intact. Moreover, the *in-vitro* release study shows that almost 78 % of montelukast and 70 % of celecoxib drugs were released at 7^{th} h of study (Figure 7). Also, bioavailability study (reported later) implies that maximum plasma drug concentrations were achieved at around 6^{th} and 8^{th} h for montelukast and celecoxib, respectively. Therefore, the anti-inflammatory activity of nanoformulation in paw edema model was almost maximum at around 6 h after carrageenan-induced inflammation or around 7 h after oral nanoformulation administration (as the

nanoformulation was administered prior to carrageenan administration). However, a detailed mechanistic study might further elaborate the mechanism.

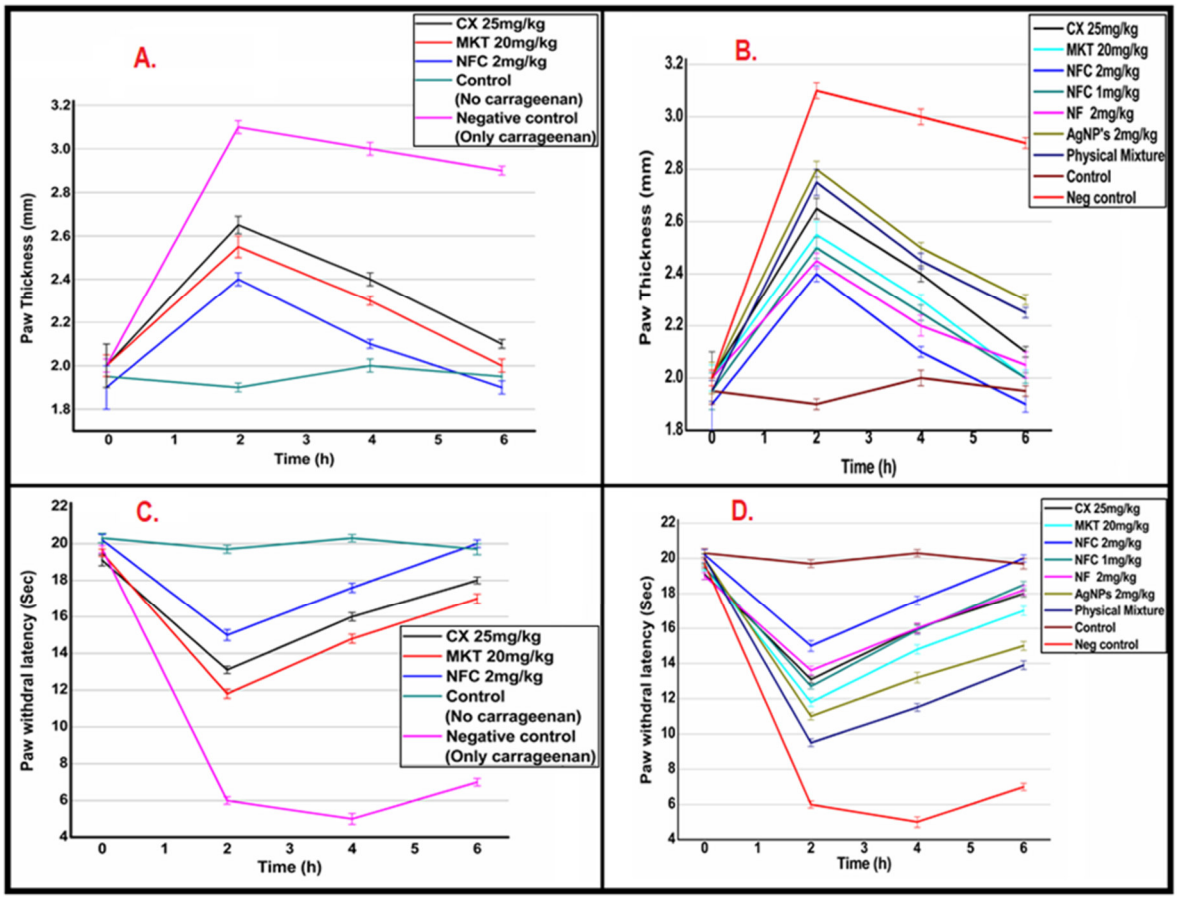

Figure 13 Anti-inflammatory effects of nanomaterials on carrageenan-induced paw edema **A**) Selected results only **B**) Detailed comparison. Potential activities of test samples in Hot plate assay (carrageenan-induced thermal hyperalgesia) **C**) Selected results only **D**) Detailed comparison.

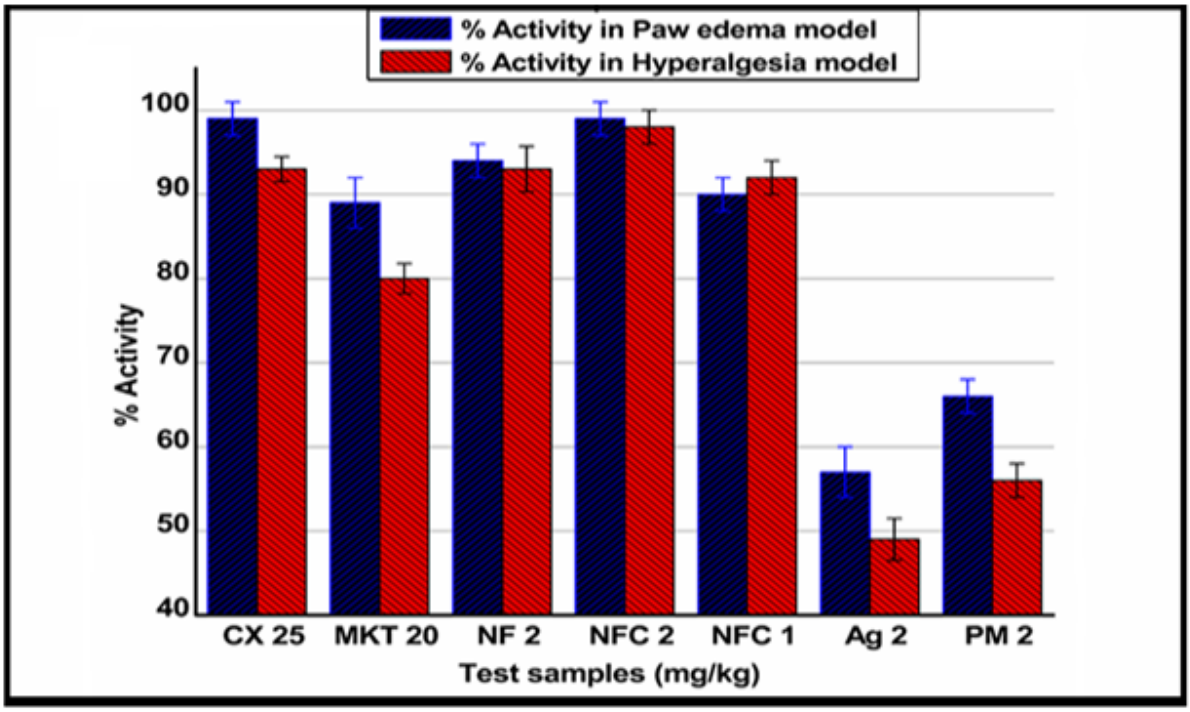

Figure 14 Percent activities of nanomaterials in Paw edema and Hyperalgesia models.

3.10.2 Effect of nanomaterials on carrageenan induced thermal hyperalgesia (Hot plate assay)

Mice were pretreated with test samples and hyperalgesic response was evaluated in an acute study by analyzing paw licking, withdrawal and jumping behaviors [64, 65, 94]. The hyperalgesic response was reduced significantly at 2 mg/kg as well as 1 mg/kg doses of NF and NFC. Pretreatment of mice with aforementioned doses avoided or suppressed inflammation impressively. Hence, improving latency time as illustrated in Figures 13C, 13D and supplementary Figure S-2B. Potential activities of test samples are compared in Figure 14 and supplementary Figure S-3B. Thermal hyperalgesia hot plate assay indicated the central analgesic actions of developed nanomaterials, whereas, the paw edema model depicted peripheral anti-inflammatory activities. These outcomes suggest that the nanomaterials are both centrally

and peripherally active [140, 141]. However, mechanistic study is required for further investigation of mechanism of action for these analgesic effects.

3.10.3 Effect of nanomaterials on brewer's yeast induced pyrexia

Antipyretic activity was evaluated through pathogen induced fever model [95, 96]. Outcomes of the study are depicted in Figures 15A, 15B and supplementary Figure S-3A. Montelukast, Celecoxib, NF and NFC exhibited impressive antipyretic effects and suppressed pyrexia significantly at 20, 25, 2 and 1 mg/kg doses, respectively. NFC at 2 mg/kg dose exhibited better antipyretic activity as compared to all other tested samples and is comparable to the effects of standard drugs at their comparatively higher doses.

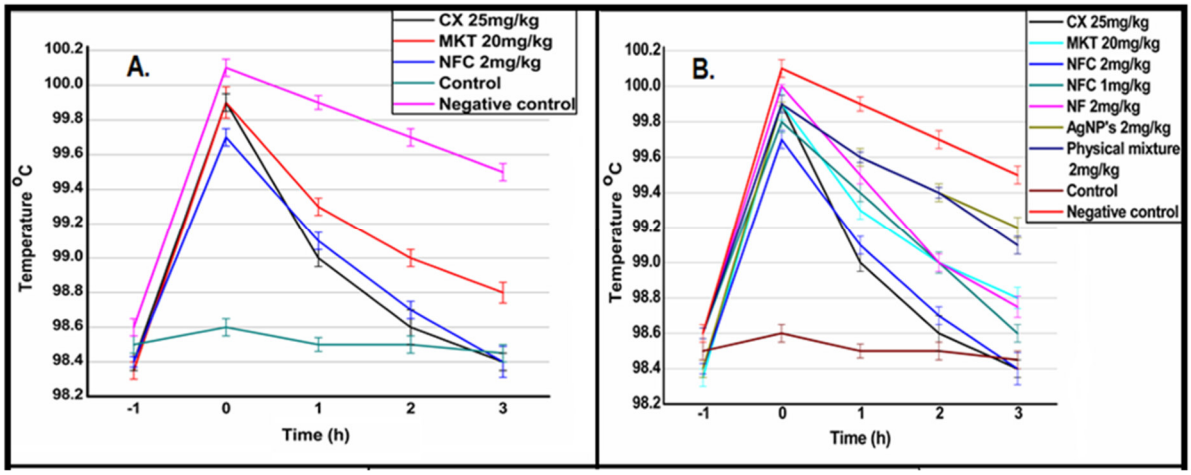

Figure 15 Potential activities of test samples against Brewer's yeast induced pyrexia **A**) Selected results only **B**) Detailed comparison.

3.10.4 Assessment of in-vivo anti-cancer activity

In-vivo anti-tumor activity was evaluated in two different xenograft mice models. Orthotopic breast adenocarcinoma model was established by injecting MCF-7 human breast adenocarcinoma cells in to fat

pads under the memory glands. Subcutaneous liver cancer xenograft mice model was developed by injecting Hep-G2 human caucasian hepatocyte carcinoma cells subcutaneously in to the flank region of albino mice. Tumors were successfully established and the treatment was started after the 3rd day of tumor mass inoculation. Mice were observed for their body weights, tumor size and toxicity symptoms. After the completion of treatment period i.e. 14th day, tumors were excised and tumor volumes were determined [98-100, 142, 143]. Tumor volume, being the most potential biomarker for cancer progress and growth, revealed the potent anti-neoplastic effect of developed nanomaterials. The results are displayed in Figure 16. NFC retarded cancer growth impressively by preventing proliferation of malignant cells. Tumor volumes and weights for control, standard and NFC were significantly distinct ($p < 0.01$) for both xenograft models (Figure 16). Percent tumor growth inhibition for orthotopic breast cancer model was determined to be 53 and 60 % for standard and NFC, respectively. Whereas, for subcutaneous Hep-G2 liver cancer model it was calculated to be 56 and 58 % for standard and NFC, respectively. Nanomaterials showed proficiency for proliferation prevention possibly because of synergistic effects of celecoxib, montelukast and AgNPs, facet modification with biocompatible polymer PVA and particle size modification (nano-sizing) [98, 100, 142, 144, 145]. Moreover, solubility enhancement of lipophilic substances minimized effective doses of anti-inflammatory drugs alleviating the associated toxicity and side effects. Results suggest promise of developed nanomaterials as hemo-compatible, potent, cheaper, less toxic oral anti-inflammatory and non-conventional anti-cancer agents. The standards used in the in-vivo studies were Tamoxifen 10 mg/kg and 5-fluorouracil 25 mg/kg. Both these drugs are conventional chemotherapeutic agents and are cytotoxic mostly for cancerous as well as normal healthy cells. Whereas, developed nanoformulation includes anti-inflammatory agents which are not cytotoxic for normal cells as they only target inflammatory pathways which are absent in normal cells. Moreover, the dose is reduced by folds e.g. 10 mg/kg of nanoformulation has better effects as compared to 25 mg/kg of 5-fluorouracil. In Figure 10, IC_{50} values of different anti-cancer agents are compared to that of nanoformulation. The IC_{50} value of nanoformulation is many folds lesser than most of the conventional cytotoxic anti-cancer agents. *In-vivo* study compared only two standard drugs still the formulation showed more potent activity.

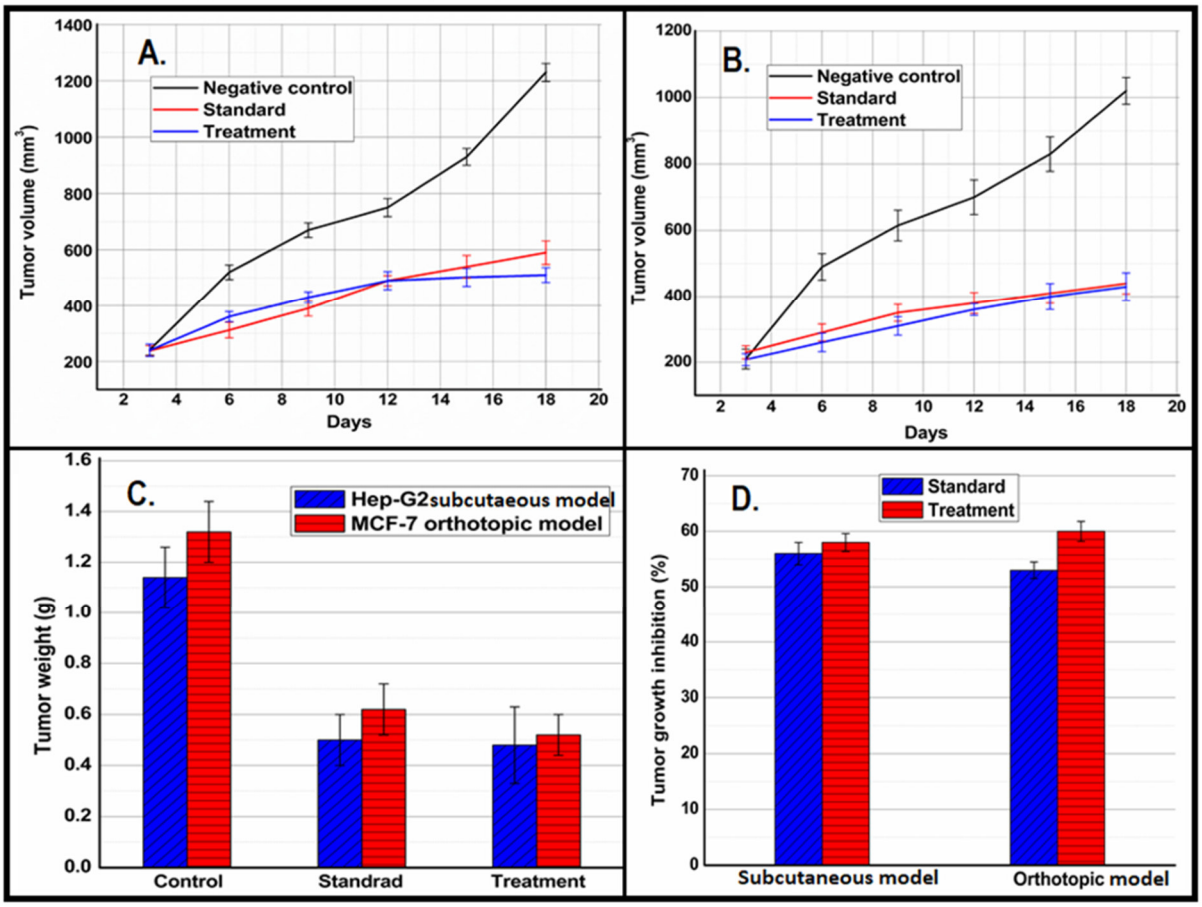

Figure 16 *In-vivo* anti-tumor activity. **A**) Tumor volume in orthotopic MCF-7 breast cancer mice model **B**) Tumor volume in orthotopic Hep-G2 liver cancer mice model **C**) Tumor weight in MCF-7 orthotopic and Hep-G2 flank cancer mice models **D**) Percent tumor growth inhibition by standard anti-cancer drugs and NCF in MCF-7 orthotopic and Hep-G2 flank cancer mice models.

3.10.5 Bioavailability study

Respective pharmacokinetic parameters were determined and are expressed in Figure 17A. Figure 17B shows mean bioavailabilities at different intervals of time. NFC depicted same pharmacokinetic trend as observed in its *in-vitro* release studies. Despite the slow and sustained release of drugs from the AgNPs, *in-vivo* anti-inflammatory effects were rapid, suggesting the uptake of intact nanoparticles (surface-modified drug conjugated AgNPs) from the gastrointestinal tract. It is beneficial in subsiding possible side effects owing to off target drug interactions and wide distribution of bare AgNPs along with providing assistance in passive tumor targeting. CX and MKT (highly lipophilic compounds) exhibit low oral bioavailability. Conjugation with AgNPs and PVA coating improved their solubility and hence bioavailability by many folds. $AUC_{0\text{-}24h}$ for NFC was significantly improved i.e. 3.8 folds for montelukast and 3.7 folds for celecoxib as compared to respective solutions. T_{max} was increased along with decreased C_{max} describing drug release from NFC in sustained manner. Modified and improved pharmacokinetics of montelukast and celecoxib may possibly be assigned to surface modification through biocompatible polymer coating providing better stability, hydrophilicity, improved dispersion, sustained release and enhanced absorption through gut. Furthermore, PVA coating might also be responsible for decreased degradation owing to biocompatibility, RES and first pass avoiding potential [52-55]. However, a detailed mechanistic study might further elaborate the possible mechanism and reasons for the outcomes.

3.10.6 Acute toxicity studies

Lethal dose (LD_{50}) determination was considered as an indicator of acute toxicity [63, 104]. Mice groups were administered with different increasing doses of NFC and then observed for 2 weeks for the food consumption, functional observations, behavior, mortality and body weight. In consideration of GHS (Globally Harmonized System) guidelines, nanoformulation, based upon its LD_{50} value, can be classified in category 3 [1, 3, 114]. An effective dose that causes lethality in 50 % of tested animal population was determined as LD_{50} and it was found out to be 65 mg/kg. The minimum effective concentration for NFC,

as observed in *in-vivo* studies, was 1 mg/kg Therefore, it is evident that the developed nanoformulation NFC exhibits wide therapeutic window. Particle size modification of AgNPs, synergism and nano-sizing reduced the minimum effective concentrations of silver and drugs, possibly further cutting back on toxicity risks and the associated side effects.

A.	Cmax (ug/ml)	Tmax (h)	Half life (t1/2) (h)	Elimination rate constant (Kel)	AUC (ug/ml.h)
NFC Montelukast (MKT)	1.45 ± 0.02	8	7	0.09	17.1
Montelukast (MKT) Solution	1.60 ± 0.03	1	5.8	0.12	4.4
NFC Celecoxib (Cx)	1.40 ± 0.03	10	10.1	0.08	19
Celecoxib (Cx) Solution	1.50 ± 0.02	1.2	8.9	0.11	5.5

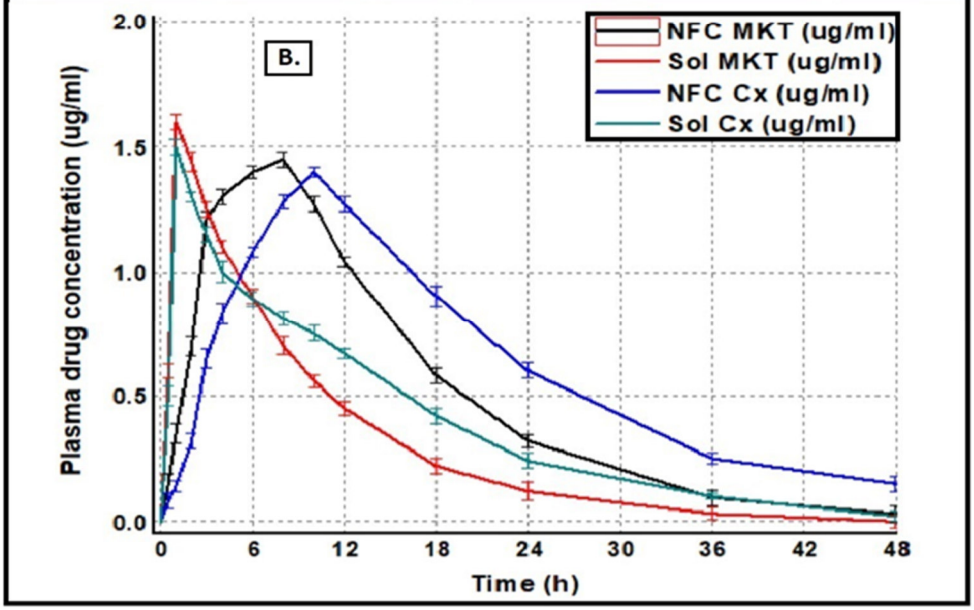

Figure 17 A) *In-vivo* pharmacokinetic parameters of NFC, CX solution and MKT solution **B)** *In-vivo* plasma drug concentrations at specified time intervals after single oral dose administration.

4. Conclusions

Inflammation plays vital role in sustaining cancer cells and halting inflammatory pathways can impede cancer growth. Non-conventional, less toxic, oral and more potent anti-cancer nanoparticles acting as

anti-inflammatory agents were successfully developed. Two anti-inflammatory agents with different mechanisms were conjugated on to anti-neoplastic silver nanoparticles (AgNPs). Nanomaterials manifested impressive anti-inflammatory activity and hence cytotoxicity against MCF-7 and Hep-G2 cancer cell lines both *in-vitro* and *in-vivo.* Conjugation of low soluble drugs to more soluble nanoparticles, surface modification with hydrophilic polymer and nanosizing improved dispersion and hence bioavailability. Surface coating with PVA provided hydrophilic nature and biocompatibility possibly avoiding reticuloendothelial system) uptake along with surface negative potential which is preferred for cellular uptake. Moreover, preferred drug release at moderately acidic conditions and targeting inflammatory pathways activated only in cancer cells provide passive tumor targeting potential. Therefore, nanoformulations manifested more efficacious and potent effects in comparison to various conventional cytotoxic agents. Non-conventional non-cytotoxic prospects associated with comparatively less and dose dependent side effects provided the advantage of negligible cytotoxicity against normal human hepatocytes (THLE-2). Multiple fold dose reduction further limited the associated side effects. Size modification of AgNPs (i.e. >100 nm), passive tumor targeting potential along with simultaneous or synergistic effects of drugs lessened their size and dose dependent toxicity risk. Successful oral delivery further provides a lead over the other therapeutic options. The nanoparticles provide a safer, potent and oral, inflammation-targeting non-conventional anti-cancer alternative to toxic conventional anti-cancer agents.

Author Contributions

All authors contributed to the conceptualization, literature search, methodology, investigation, writing—original draft preparation, and writing—review and editing. All authors have read and agreed to the published version of the manuscript.

Funding

This research received funding from HEC indigenous scholarship [17-5(2MD3-045], Pakistan. Synthesis and characterization part was conducted at National Center for Physics (NCP), Islamabad.

Institutional Review Board Statement

All surgical and test procedures on the animals were conducted under approval of the Bio-Ethical Committee of Quaid-i-Azam University, Islamabad, Pakistan (Protocol #BEC-FBS-QAU2020-214) in accordance with the internationally accepted principles for laboratory animal use.

Informed Consent Statement

Not applicable.

Data Availability Statement

Data available in the study

Electronic Supplementary Material

Supplementary material (Figures S-1, S-2 and S-3) is available in the online version of this article.

Conflict of interests

The authors have no potential conflict of interest.

References

1. Rehman, F. U.; Mazhar, K.; Malik, A.; Sohaila Naz, S.; UllahShah, K.; Khan, A.; Khan, S.; Ahmed, R.; Qaisar, S. Surface modified multifaceted nanocarriers for oral non-conventional cancer therapy; synthesis and evaluation. *Mater. Sci. Eng. C* **2021**, 123, 111940.
2. Rehman, F. U.; Shah, K. U.; Shah, S. U.; Khan, I. U.; Khan, G. M.; Khan, A. From nanoemulsions to self-nanoemulsions, with recent advances in self-nanoemulsifying drug delivery systems (SNEDDS). *Exp. Opin. Drug Delivery* **2017**, 14(11), 1325-1340.
3. Rahdar, A.; Taboada, P.; Hajinezhad, M. R.; Barani, M.; Beyzaei, H. Effect of tocopherol on the properties of Pluronic F127 microemulsions: Physico-chemical characterization and in vivo toxicity. *J. Mol. Liquids* **2019**, 277, 624-630.
4. DeSantis, C. E.; Lin, C. C.; Mariotto, A. B.; Siegel, R. L.; Stein, K. D.; Kramer, J. L.; Alteri, R.; Robbins, A. S.; Jemal, A. Cancer treatment and survivorship statistics, 2014. *CA: Cancer J Clin*. **2014**, 64(4), 252-271.
5. Pirmohamed, M.; James, S.; Meakin, S.; Green, C.; Scott, A. K.; Walley, T. J.; Farrar, K.; Park, B. K.; Breckenridge, A. M. Adverse drug reactions as cause of admission to hospital: prospective analysis of 18 820 patients. *BMJ* **2004**, 329(7456), 15-19.
6. Lazarou, J.; Pomeranz, B. H.; Corey, P. N. Incidence of adverse drug reactions in hospitalized patients: a meta-analysis of prospective studies. *JAMA* **1998**, 279(15), 1200-1205.
7. Hassett, M. J.; O'Malley, A. J.; Pakes, J. R.; Newhouse, J. P.; Earle, C. C. Frequency and cost of chemotherapy-related serious adverse effects in a population sample of women with breast cancer. *J. Natl. Cancer Inst*. **2006**, 98(16), 1108-1117.
8. Borovski, T.; De Sousa E Melo, F.; Vermeulen, L.; Medema, J. P. Cancer stem cell niche: the place to be. *Cancer Res*. **2011**, 71(3), 634-639.
9. Kuhn, N. Z.; Tuan, R. S. Regulation of stemness and stem cell niche of mesenchymal stem cells: implications in tumorigenesis and metastasis. *Journal Cell. Physiol*. **2010**, 222(2), 268-277.

10. Fuchs, E.; Tumbar, T.; Guasch, G.; Socializing with the neighbors: stem cells and their niche. *Cell* **2004**, 116(6), 769-778.

11. Crusz, S. M.; Balkwill, F. R. Inflammation and cancer: advances and new agents. *Nature Rev. Clini. Oncology* **2015**, 12(10), 584-596.

12. Frölich, J. A classification of NSAIDs according to the relative inhibition of cyclooxygenase isoenzymes. *Trends Pharmacol. Sci*. **1997**, 18(1), 30-34.

13. Ding, N.; Maiuri, A. R.; O'Hagan, H. M. The emerging role of epigenetic modifiers in repair of DNA damage associated with chronic inflammatory diseases. *Mutation Res. Rev. Mutation Res*. **2019**, 780, 69-81.

14. Chiba, T.; Marusawa, H.; Ushijima, T. Inflammation-associated cancer development in digestive organs: mechanisms and roles for genetic and epigenetic modulation. *Gastroenterology* **2012**, 143(3), 550-563.

15. Rothwell, P. M.; Price, J. F.; Fowkes, F. G. R.; Zanchetti, A.; Roncaglioni, M. C.; Tognoni, G.; Lee, R.; Belch, J. F. F.; Wilson, M.; Mehta, Z.; Meade, T. W. Short-term effects of daily aspirin on cancer incidence, mortality, and non-vascular death: analysis of the time course of risks and benefits in 51 randomised controlled trials. *The Lancet* **2012**, 379(9826), 1602-1612.

16. Ungefroren, H.; Sebens, S.; Seidl, D.; Lehnert, H.; Hass, R. Interaction of tumor cells with the microenvironment. *Cell Comm. Signaling* **2011**, 9(1), 1-8.

17. Dizdaroglu, M.; Oxidatively induced DNA damage: mechanisms, repair and disease. *Cancer Lett*. **2012**, 327(1-2), 26-47.

18. Kawanishi, S.; Ohnishi, S.; Ma, N.; Hiraku, Y.; Oikawa, S.; Murata, M. Nitrative and oxidative DNA damage in infection-related carcinogenesis in relation to cancer stem cells. *Genes Environ.* **2016**, 38(1), 26.

19. Nishida, N.; Kudo, M. Oxidative stress and epigenetic instability in human hepatocarcinogenesis. *Digest. Dis*. **2013**, 31(5-6), 447-453.

20. Deeks, S. G. HIV infection, inflammation, immunosenescence, and aging. *Ann. Rev. Med*. **2011**, 62, 141-155.

21. Nasi, M.; Pinti, M.; Mussini, C.; Cossarizza, A. Persistent inflammation in HIV infection: established concepts, new perspectives. *Immun. Lett*. **2014**, 161(2), 184-188.

22. Elbi, S.; Nimal, T. R.; Rajan, V. K.; Baranwal, G.; Biswas, R.; Jayakumar, R.; Sathianarayanan, S. Fucoidan coated ciprofloxacin loaded chitosan nanoparticles for the treatment of intracellular and biofilm infections of Salmonella. *Coll. Surf. B Biointerfaces* **2017**, 160, 40-47.

23. Makroo, R. N.; Raina, V.; Bhatia, A.; Gupta, R.; Majid, A.; Thakur, U. K.; Rosamma, N. L. Evaluation of the red cell hemolysis in packed red cells during processing and storage. *Asian J. Transf. Sci*. **2011**, 5(1), 15.

24. Jutel, M.; Agache, I.; Bonini, S.; Burks, A. W.; Calderon, M.; Canonica, W.; Cox, L.; Demoly, P.; Frew, A. J.; O'Hehir, R.; et al. International consensus on allergy immunotherapy. *J. Allergy Clin. Immunol*. **2015**, 136(3), 556-568

25. Claria, J.; Romano, M. Pharmacological intervention of cyclooxygenase-2 and 5-lipoxygenase pathways. Impact on inflammation and cancer. *Curr. Pharm. Des*. **2005**, 11(26), 3431-3447.

26. Gately, S.; Li, W. W. Multiple roles of COX-2 in tumor angiogenesis: a target for antiangiogenic therapy. *Semin. Oncology*. **2004**, 31(7), 2-11.

27. Elder, D. J.; Halton, D. E.; Hague, A.; Paraskeva, C. Induction of apoptotic cell death in human colorectal carcinoma cell lines by a cyclooxygenase-2 (COX-2)-selective nonsteroidal anti-inflammatory drug: independence from COX-2 protein expression. *Clin. Cancer Res*. **1997**, 3(10), 1679-1683.

28. Celotti, F.; Durand, T. The metabolic effects of inhibitors of 5-lipoxygenase and of cyclooxygenase 1 and 2 are an advancement in the efficacy and safety of anti-inflammatory therapy. *Prostaglandin Other Lipid Med.*. **2003**, 71(3-4), 147-162.

29. Mason, R. P.; Mary, F. W.; McNulty, H. P.; Lockwood, S. F.; Byun, J.; Day, C. A.; Jacob, R. F. Rofecoxib increases susceptibility of human LDL and membrane lipids to oxidative damage: a mechanism of cardiotoxicity. *J. Cardiovasc. Pharmacol*. **2006**, 47, S7-S14.

30. Barnabe, C.; Martin, B. J.; Ghali, W. A. Systematic review and meta-analysis: anti–tumor necrosis factor α therapy and cardiovascular events in rheumatoid arthritis. *Arthritis Care Res*. **2011**. 63(4), 522-529.

31. Dajani, E.; Islam, K. Cardiovascular and gastrointestinal toxicity of selective cyclo-oxygenase-2 inhibitors in man. *J. Physiol. Pharmacol*. **2008**. 59(Suppl 2), 117-133.

32. Hernández-Díaz, S.; Varas-Lorenzo, C.; García Rodríguez, L. A. Non-steroidal antiinflammatory drugs and the risk of acute myocardial infarction. *Basic Clin. Pharmacol. Toxicol*. **2006**, 98(3), 266-274.

33. Ng, S.C.; Chan, F. K. L. NSAID-induced gastrointestinal and cardiovascular injury. *Curr. Opin. Gastroenterol*. **2010**, 26(6), 611-617.

34. Da Costa, B. R.; Reichenbach, S.; Keller, N.; Nartey, L.; Wandel, S.; Jüni, P.; Trelle, S. Effectiveness of non-steroidal anti-inflammatory drugs for the treatment of pain in knee and hip osteoarthritis: a network meta-analysis. *Lancet* **2017**, 390(10090), e21-e33.

35. Barker, H.E.; Cox, T. R.; Erler, J. T. The rationale for targeting the LOX family in cancer. *Nature Rev. Cancer* **2012**, 12(8), 540-552.

36. Ding, X.-Z.; Iversen, P.; Cluck, M. W.; Knezetic, J. A.; Adrian, T. E. Lipoxygenase inhibitors abolish proliferation of human pancreatic cancer cells. *Biochem. Biophys. Res. Comm*. **1999**, 261(1), 218-223.

37. Levy, B. D.; De Sanctis, G. T.; Devchand, P. R.; Kim, E.; Ackerman, K.; Schmidt, B. A.; Szczeklik, W.; Drazen, J. M.; Serhan, C. N. Multi-pronged inhibition of airway hyper-responsiveness and inflammation by lipoxin A 4. *Nature Med*. **2002**, 8(9), 1018-1023.

38. Shureiqi, I.; Chen, D.; Lee, J. J.; Yang, P.; Newman, R. A.; Brenner, D. E.; Lotan, R.; Fischer, S. M.; Lippman, S. M. 15-LOX-1: a novel molecular target of nonsteroidal anti-inflammatory drug-induced apoptosis in colorectal cancer cells. *J. Natl. Cancer Inst*. **2000**, 92(14), 1136-1142.

39. Ye, Y. N.; Wu, W. K. K.; Shin, V. Y.; Bruce, I. C.; Wong, B. C. Y.; Cho, C. H. Dual inhibition of 5-LOX and COX-2 suppresses colon cancer formation promoted by cigarette smoke. *Carcinogenesis* **2005**, 26(4), 827-834.

40. Yoshimura, R.; Matsuyama, M.; Mitsuhashi, M.; Takemoto, Y.; Tsuchida, K.; Kawahito, Y.; Sano, H.; Nakatani, T. Relationship between lipoxygenase and human testicular cancer. *Int. J. Mol. Med*. **2004**, 13(3), 389-393.

41. Goossens, L.; Pommery, N.; Pierre Henichart, J. COX-2/5-LOX dual acting anti-inflammatory drugs in cancer chemotherapy. *Curr. Topics Med. Chem*. **2007**, 7(3), 283-296.

42. Wang, D.; DuBois, R. N. The role of COX-2 in intestinal inflammation and colorectal cancer. *Oncogene* **2010**, 29(6), 781-788.

43. Salehi, S.; Shandiz, S. A. S.; Ghanbar, F.; Darvish, M. R.; Ardestani, M. S.; Mirzaie, A.; Jafari, M. Phytosynthesis of silver nanoparticles using Artemisia marschalliana Sprengel aerial part extract and assessment of their antioxidant, anticancer, and antibacterial properties. *Int. J. Nanomed*. **2016**, 11, 1835.

44. Gurunathan, S.; Lee, K.-J.; Kalishwaralal, K.; Sheikpranbabu, S.; Vaidyanathan, R.; Eom, S. H. Antiangiogenic properties of silver nanoparticles. *Biomaterials* **2009**, 30(31), 6341-6350.

45. Kalishwaralal, K.; Banumathi, E.; Pandian, S. R. K.; Deepak, V.; Muniyandi, J.; Eom, S. H.; Gurunathan, S. Silver nanoparticles inhibit VEGF induced cell proliferation and migration in bovine retinal endothelial cells. *Coll. Surf. B Biointerfaces* **2009**, 73(1), 51-57.

46. Panyala, N.R.; Peña-Méndez, E.M.; Havel, J. Silver or silver nanoparticles: a hazardous threat to the environment and human health? *J. Appl. Biomed*. **2008**, 6(3), 117-129.

47. Oei, J.D.; Zhao, W. W.; Chu, L.; DeSilva, M. N.; Ghimire, A.; Rawls, H. R.; Whang, K. Antimicrobial acrylic materials with in situ generated silver nanoparticles. *J. Biomed. Mater. Res. B Appl. Biomater*. **2012**, 100(2), 409-415.

48. Evans, E.R.; Bugga, P. Asthana, V.; Drezek, R. Metallic nanoparticles for cancer immunotherapy. *Mater. Today* **2018**, 21(6), 673-685.

49. Budama-Kilinc, Y.; Cakir-Koc, R.; Zorlu, T.; Ozdemir, B.; Karavelioglu, Z.; Egil, A. C.; Kecel-Gunduz, S. Assessment of Nano-toxicity and Safety Profiles of Silver Nanoparticles. Silver nanoparticles-fabrication, characterization and applications. *IntechOpen: London* **2018**, 185.

50. Cho, Y.-M.; Mizuta, Y.; Akagi, J.-I.; Toyoda, T.; Sone, M.; Ogawa, K. Size-dependent acute toxicity of silver nanoparticles in mice. *J. Toxicol. Pathol*. **2018**, 31(1), 73-80.

51. Don, T.-M.; King, C.-F.; Chiu, W.-Y.; Peng, C.-A. Preparation and characterization of chitosan-g-poly (vinyl alcohol)/poly (vinyl alcohol) blends used for the evaluation of blood-contacting compatibility. *Carbohydrate Polym*. **2006**, 63(3), 331-339.

52. Shagholani, H.; Ghoreishi, S. M.; Mousazadeh, M. Improvement of interaction between PVA and chitosan via magnetite nanoparticles for drug delivery application. *Int. J. Biol. Macromol*. **2015**, 78, 130-136.

53. Mohapatra, S.; Pramanik, N.; Ghosh, S. K.; Pramanik, P. Synthesis and characterization of ultrafine poly (vinylalcohol phosphate) coated magnetite nanoparticles. *J. Nanosci. Nanotechnol*. **2006**, 6(3), 823-829.

54. Kurchania, R.; Sawant, S. S.; Ball, R. J. Synthesis and characterization of magnetite/polyvinyl alcohol core–shell composite nanoparticles. *J. Am. Ceram. Soc*. **2014**, 97(10), 3208-3215.

55. Chen, Q.; Cabanas-Polo, S.; Goudouri, O.-M.; Boccaccini, A. R. Electrophoretic co-deposition of polyvinyl alcohol (PVA) reinforced alginate–Bioglass® composite coating on stainless steel: Mechanical properties and in-vitro bioactivity assessment. *Mater. Sci. Eng. C* **2014**, 40, 55-64.

56. Hillaireau, H.; Couvreur, P. Nanocarriers' entry into the cell: relevance to drug delivery. *Cell. Mol. Life Sci*. **2009**, 66(17), 2873-2896.

57. Mortensen, L. J.; Oberdörster, G.; Pentland, A. P.; DeLouise, L. A. In vivo skin penetration of quantum dot nanoparticles in the murine model: the effect of UVR. *Nano Lett.*. **2008**, 8(9), 2779-2787.

58. Shi, X.; Thomas, T. P.; Myc, L. A.; Kotlyar, A. Baker, J. R. Jr Synthesis, characterization, and intracellular uptake of carboxyl-terminated poly (amidoamine) dendrimer-stabilized iron oxide nanoparticles. *Phys. Chem. Chem. Phys*. **2007**, 9(42), 5712-5720.

59. Patil, S.; Sandberg, A.; Heckert, E.; Self, W.; Seal, S. Protein adsorption and cellular uptake of cerium oxide nanoparticles as a function of zeta potential. *Biomaterials* **2007**, 28(31), 4600-4607.

60. Wilhelm, C., Billotey, C.; Roger, J.; Pons, J. N.; Bacri, J.-C.; Gazeau, F. Intracellular uptake of anionic superparamagnetic nanoparticles as a function of their surface coating. *Biomaterials* **2003**, 24(6), 1001-1011.

61. Zhu, J.; Huang, J.-W.; Tseng, P.-H.; Yang, Y.-T.; Fowble, J.; Shiau, C.-W.; Shaw, Y.-J.; Kulp, S. K.; Chen, C.-S. From the cyclooxygenase-2 inhibitor celecoxib to a novel class of 3-phosphoinositide-dependent protein kinase-1 inhibitors. *Cancer Res*. **2004**, 64(12), 4309-4318.

62. Hilvo, M.; Innocenti, A.; Monti, S. M.; Simone, G. D.; Supuran, C. T.; Parkkila, S. Recent advances in research on the most novel carbonic anhydrases, CA XIII and XV. *Curr. Pharm. Des*. **2008**, 14(7), 672-678.

63. Ahmed, M. Acute toxicity (lethal dose 50 calculation) of herbal drug Somina in rats and mice. *Pharmacol. Pharm*. **2015**, 6(03), 185.

64. Naveed, M.; Khan, S. Z.; Zeeshan, S.; Khan, A.; Shal, B.; Atiq, A.; Ali, H.; Ullah, R.; Zia-ur-Rehman; Khan, S. A new cationic palladium (II) dithiocarbamate exhibits anti-inflammatory, analgesic, and antipyretic activities through inhibition of inflammatory mediators in in vivo models. *Naunyn-Schmiedeberg's Arch. Pharmacol*. **2019**, 392(8), 961-977.

65. Ravi Kanth, V.; Diwan, P. V. Analgesic, antiinflammatory and hypoglycaemic activities of Sida cordifolia. *Phytother. Res*. **1999**, 13(1), 75-77.

66. Dave, V.; Gupta, A.; Singh, P.; Gupta, C.; Sadhu, V.; Reddy, K. R. Synthesis and characterization of celecoxib loaded PEGylated liposome nanoparticles for biomedical applications. *Nano-Struct. Nano-Objects* **2019**, 18, 100288.

67. Im, S. H.; Jung, H. T.; Ho, M. J.; Lee, J. E.; Kim, H. T.; Kim, D. Y.; Lee, H. C.; Choi, Y. S.; Kang, M. J. Montelukast Nanocrystals for Transdermal Delivery with Improved Chemical Stability. *Pharmaceutics* **2020**, 12(1), 18.

68. Turkevich, J.; Cooperá Stevenson, P.; Hillier, J. A study of the nucleation and growth processes in the synthesis of colloidal gold. *Discuss. Faraday Soc.* **1951**, 11, 55–75.

69. Muhammad, Z.; Raza, A.; Ghafoor, S.; Naeem, A.; Naz, S. S.; Riaz, S.; Ahmed, W.; Rana, N. F. PEG capped methotrexate silver nanoparticles for efficient anticancer activity and biocompatibility. *Eur. J. Pharm. Sci*. **2016**, 91, 251-255.

70. Naz, S. S.; Shah, M. R.; Islam, N. U.; Alam, S. S. Enhanced urease inhibition activity of Ag nanomaterials capped with N-substituted methyl 5-acetamido-β-resorcylate. *Prog. Nat. Sci. Mater. Int*. **2019**, 29(2), 129-137.

71. Ahmed, R.; Baig, M. A. A comparative study of single and double pulse laser induced breakdown spectroscopy. *J. Appl. Phys*. **2009**, 106(3), 033307.

72. Akhtar, M.; Jabbar, A.; Mehmood, S.; Ahmed, N.; Ahmed, R.; Baig, M. A. Magnetic field enhanced detection of heavy metals in soil using laser induced breakdown spectroscopy. *Spectrochim. Acta B: Atom. Spectr*. **2018**, 148, 143-151.

73. Iqbal, J.; Ahmed, R.; Rafique, M.; Anwar-ul-Haq, M.; Baig, M. A. Spatial diagnostics of the laser-produced tin plasma in air. *Laser Phys*. **2016**, 26(7), 076001.

74. Jabbar, A.; Akhtar, M.; Mehmmod, S.; Iqbal, M.; Ahmed, R.; Baig, M. A. Quantification of copper remediation in the Allium cepa L. leaves using electric field assisted laser induced breakdown spectroscopy. *Spectrochim. Acta B Atom. Spectr*. **2019**, 162, 105719.

75. Naz, M.; Qureshi, M. Z.; Shahbaz, A.; Haider, A.; Ikram, M.; Nafees, M.; Shahzadi, A.; Bashir, T.; Ali, S.; Blackburn, A. C.; Chen, H.; Tricoli, A.et al., Bio-inspired synthesis of silver nanoparticles: anticancer drug carrier, catalytic and bactericidal potential. *Nanosci. Nanotechnol. Lett*. **2018**, 10(7), 889-899.

76. *British Pharmacopoeia*. Vol. I. 2017, London.

77. Azizi, M.; Ghourchian, H.; Yazdian, F.; Bagherifam, S.; Bekhradnia, S.; Nyström, B. Anti-cancerous effect of albumin coated silver nanoparticles on MDA-MB 231 human breast cancer cell line. *Sci. Rep.* **2017**, 7(1), 5178.

78. Karthik, I.; Bharath Rathna Kumar, P.; Venu Priya, R.; Sunil Kumar, K.; Ranjith Singh Rathore, B. Evaluation of anti-inflammatory activity of canthium parviflorum by in-vitro method. *Indian J. Res. Pharm. Biotechnol*. **2013**, 1(5), 729-731

79. Leelaprakash, G.; Dass, S. M. Invitro anti-inflammatory activity of methanol extract of Enicostemma axillare. *Int. J. Drug Dev. Res*. **2011**, 3(3), 189-196.

80. Xu, H.; Yao, N.; Xu, H.; Wang, T.; Li, G.; Li, Z. Characterization of the interaction between eupatorin and bovine serum albumin by spectroscopic and molecular modeling methods. *Int. J. Mol. Sci*. **2013**, 14(7), 14185-14203.

81. Seifert, A.; Rawel, H. M.; Kroll, J.; Harding, S. E. Characterization of bovine serum albumin/chlorogenic acid solution mixtures by analytical ultracentrifugation. *Anal. Ultracentrifug. VII*. **2004**, 83-88.

82. Rahman, H.; Eswaraiah, M. C.; Dutta, A. In-vitro anti-inflammatory and anti-arthritic activity of Oryza Sativa Var. joha rice (an aromatic indigenous rice of Assam). *Am. Eurasian J. Agric. Environ. Sci*. **2015**, 15, 115-121.

83. Onasanya, A.; Adewale, O. B.; Obafemi, T. O.; Ojo, A. A. Comparison of Protein Yields of Four Protein Extraction Methods from Leaf and Seed of Moringa oleifera. *Int. J. Appl. Res. Technol*. **2015**, 4(7), 98-109.

84. Fisher, G. A.; Sikic, B. I. Clinical studies with modulators of multidrug resistance. *Hematol. Oncology Clin. North Am*. **1995**, 9(2), 363-382.

85. Bano, S.; Nazir, S.; Munir, S.; AlAjmi, M. F.; Afzal, M.; Mazhar, K. “Smart” nickel oxide based core–shell nanoparticles for combined chemo and photodynamic cancer therapy. *Int. J. Nanomed*. **2016**, 11, 3159.

86. Hakami, T. M.; Davarpanah, A. M.; Rahdar, A.; Barrett, S. D. Structural and magnetic study and cytotoxicity evaluation of tetra-metallic nanoparticles of Co0. 5Ni0. 5CrxFe2-xO4 prepared by co-precipitation. *J. Mol. Struct*. **2018**, 1165, 344-348.

87. Kiruthika, V.; Maya, S.; Suresh, M. K.; Kumar, V. A.; Jayakumar, R.; Biswas, R. Comparative efficacy of chloramphenicol loaded chondroitin sulfate and dextran sulfate nanoparticles to treat intracellular Salmonella infections. *Coll. Surf. B Biointerfaces* **2015**, 127, 33-40.

88. Maya, S.; Indulekha, S.; Sukhithasri, V.; Smith, K. T.; Nair, S. V.; Jayakumar, R.; Biswas, R. Efficacy of tetracycline encapsulated O-carboxymethyl chitosan nanoparticles against intracellular infections of Staphylococcus aureus. *Int. J. Biol. Macromol.* **2012**, 51(4), 392-399.

89. Dhanalakshmi, V.; Nimal, T. R.; Sabitha, M.; Biswas, R.; Jayakumar, R. Skin and muscle permeating antibacterial nanoparticles for treating Staphylococcus aureus infected wounds. *J. Biomed. Mater. Res. B Appl. Biomater*. **2016**, 104(4), 797-807.

90. Al-Ghamdi, M. S. The anti-inflammatory, analgesic and antipyretic activity of Nigella sativa. *J. Ethnopharmacol*. **2001**, 76(1), 45-48.

91. Chi, S.-C.; Jun, H. W. Anti-inflammatory activity of ketoprofen gel on carrageenan-induced paw edema in rats. *J. Pharm. Sci*. **1990**, 79(11), 974-977.

92. El-Ela, F. I. A.; El-Banna, H. Exploring novel medical applications for commonly used veterinary drug (tilmicosin antibiotic). *Insights Vet. Sci*. **2017**, 1, 1-16.

93. Eddy, N. B.; Leimbach, D. Therapeutics, Synthetic analgesics. II. Dithienylbutenyl-and dithienylbutylamines. *J. Pharm. Exp. Therap.* **1953**, 107(3), 385-393.

94. Ullah, M. Z.; Khan, A. U.; Afridi, R.; Rasheed, H; Khalid, S.; Naveed, M.; Ali, H.; Kim, Y. S.; Khan, S. Attenuation of inflammatory pain by puerarin in animal model of inflammation through inhibition of pro-inflammatory mediators. *Int. Immunopharmacol*. **2018**, 61, 306-316.

95. Hossain, E.; Mandal, S. C.; Gupta, J. K. Phytochemical screening and in-vivo antipyretic activity of the methanol leaf-extract of Bombax malabaricum DC (Bombacaceae). *Trop. J. Pharm. Res*. **2011**, 10(1), 55-60.

96. Sultana, S.; Akhtar, N.; Asif, H. M. Phytochemical screening and antipyretic effects of hydro-methanol extract of Melia azedarach leaves in rabbits. *Bangladesh J. Pharmacol*. **2013**, 8(2), 214-217.

97. Seifaddinipour, M.; Farghadani, R; Namvar, F.; Mohamad, J. B.; Muhamad, N. A. In vitro and in vivo anticancer activity of the most cytotoxic fraction of pistachio hull extract in breast cancer. *Molecules* **2020**, 25(8), 1776.

98. Paschall, A. V.; Liu, K. An orthotopic mouse model of spontaneous breast cancer metastasis. *J. Visual. Exp*. **2016**, (114), 54040.

99. Li, H., Haiyan Li; Wang, Q.; Dong, L.; Liu, C.; Sun, Z.; Gao, L.; Wang, X. Morusin suppresses breast cancer cell growth in vitro and in vivo through C/EBPβ and PPARγ mediated lipoapoptosis. *J. Exp. Clin. Cancer Res*. **2015**, 34(1), 1-12.

100. Jeyaprakash, K.; AlSalhi, M. S.; Devanesan, S. Anticancer and antioxidant efficacy of silver nanoparticles synthesized from fruit of Morinda citrifolia Linn on Ehrlich ascites carcinoma mice. *J. King Saud Univ. Sci*. **2020**, 32(7), 3181-3186.

101. Wankhede, S.; Kumar, N.; Simon, L.; Biswas, S.; Gourishetti, K.; Ramalingayya, G. V.; Joshi, M.; Rao, C. M. Evaluation of in vitro and in vivo anticancer potential of two 5-acetamido chalcones against breast cancer. *EXCLI J*. **2017**, 16, 1150.

102. *British Pharmacopoeia*. Vol. II. 2017, London.

103. Han, D.-G.; Kwak, J.; Seo, S.-W.; Kim, J.-M.; Yoo, J.-W.; Jung, Y.; Lee, Y.-H.; Kim, M.-S.; Jung, Y.-S.; Yun, H.; Yoon, I.-S. Pharmacokinetic evaluation of metabolic drug interactions between repaglinide and celecoxib by a bioanalytical HPLC method for their simultaneous determination with fluorescence detection. *Pharmaceutics* **2019**, 11(8), 382.

104. Venancio, A.M.; Onofre, A. S. C.; Lira, A. F.; Alves, P. B.; Blank, A. F.; Antoniolli, Â. R.; Marchioro, M.; dos Santos Estevam, C.; de Araujo, B. S. Chemical composition, acute toxicity, and

antinociceptive activity of the essential oil of a plant breeding cultivar of basil (Ocimum basilicum L.). *Planta Med*. **2011**, 77(08), 825-829.

105. Hasanein, P.; Rahdar, A.; Esmaeilzadeh Bahabadi, S.; Kumar, A.; Kyzas, G. Z. Manganese/cerium nanoferrites: Synthesis and toxicological effects by intraperitoneal administration in rats. *Inorg. Chem. Comm*. **2021**, 125, 108433.

106. Hamama, A.K.; Ray, J.; Day, R. O.; Brien, J. E. Simultaneous Determination of rofecoxib and celecoxib in human plasma by high-performance liquid chromatography. *J. Chromatographic Sci*. **2005**, 43(7), 351-354.

107. Attimarad, M.; Narayanswamy, V. K.; Aldhubaib, B. E.; Sreeharsha, N.; Nair, A. B. Development of UV spectrophotometry methods for concurrent quantification of amlodipine and celecoxib by manipulation of ratio spectra in pure and pharmaceutical formulation. *PloS One* **2019**, 14(9), e0222526.

108. Homayouni, A.; Sadeghi, F.; Nokhodchi, A.; Varshosaz, J.; Garekani, H. A. Preparation and characterization of celecoxib solid dispersions; comparison of poloxamer-188 and PVP-K30 as carriers. *Iran. J. Basic Med. Sci*. **2014**, 17(5), 322.

109. Jo, K.; Cho, J. M.; Lee, H.; Kim, E. K.; Kim, H. C.; Kim, H.; Lee, J. Enhancement of aqueous solubility and dissolution of celecoxib through phosphatidylcholine-based dispersion systems solidified with adsorbent carriers. *Pharmaceutics* **2019**, 11(1), 1.

110. Aferni, A. E. L.; Guettari, M.; Tajouri, T.; Rahdar, A. The confinement of PVP in AOT microemulsions: Effect of water content and PVP concentration regime on electrical percolation phenomenon. *J. Mol. Liquids* **2020**, 318, 114012.

111. Crivelli, B.; Bari, E.; Perteghella, S.; Catenacci, L.; Sorrenti, M.; Mocchi, M.; Faragò, S.; Tripodo, G.; Prina-Mello, A.; Torre, M. L. Silk fibroin nanoparticles for celecoxib and curcumin delivery:

ROS-scavenging and anti-inflammatory activities in an in vitro model of osteoarthritis. *European J. Pharm. Biopharm*. **2019**, 137, 37-45.

112. Pillai, A.M.; Sivasankarapillai, V. S.; Rahdar, A.; Joseph, J.; Sadeghfar, F.; Anuf A, R.; Rajesh, K.; Kyzas, G. Z. Green synthesis and characterization of zinc oxide nanoparticles with antibacterial and antifungal activity*. J. Mol. Struct*. **2020**, 1211, 128107.

113. Priyanka, K.; Hasan, S. A. A. Preparation and evaluation of montelukast sodium loaded solid lipid nanoparticles. *J. Young Pharm*. **2012**, 4(3), 129-137.

114. Saravanan, M.; Siva kumari, K.; Pratap Reddy, P.; Naidu, M. N.; Moses Babu, J.; Srivastava, A. K.; Lakshmi Kumar, T.; Chandra Sekhar, B. V. V. N.; Satyanarayana, B. Identification, synthesis, isolation and spectral characterization of potential impurities of montelukast sodium. *J. Pharm. Biomed. Anal*. **2008**, 48(3), 708-715.

115. Rehman, F. U.; Mazhar, K.; Malik, A.; Sohaila Naz, S.; UllahShah, K.; Khan, A.; Khan, S.; Ahmed, R.; Qaisar, S. Surface modified multifaceted nanocarriers for oral non-conventional cancer therapy; synthesis and evaluation. *Mater. Sci. Eng. C* 2021, 123, 111940.

116. Mansur, H.S.; Sadahira, C. M.; Souza, A. N.; Mansur, A. A. P. FTIR spectroscopy characterization of poly (vinyl alcohol) hydrogel with different hydrolysis degree and chemically crosslinked with glutaraldehyde. *Mater. Sci. Eng. C*. **2008**, 28(4), 539-548.

117. Kim, T.-H.; Kim, M.; Park, H.-S.; Shin, U. S.; Gong, M.-S.; Kim, H.-W. Size-dependent cellular toxicity of silver nanoparticles. *J. Biomed. Mater. Res. A* **2012**, 100(4), 1033-1043.

118. Park, M. V. D. Z.; Neigh, A. M.; Vermeulen, J. P.; de la Fonteyne, L. J. J.; Verharen, H. W.; Briedé, J. J.; Loveren, H.; de Jong, W. H. The effect of particle size on the cytotoxicity, inflammation, developmental toxicity and genotoxicity of silver nanoparticles. *Biomaterials* **2011**, 32(36), 9810-9817.

119. Ha, E.-S.; Choo, G.-H.; Baek, I.-H.; Kim, M.-S. Formulation, characterization, and in vivo evaluation of celecoxib-PVP solid dispersion nanoparticles using supercritical antisolvent process. *Molecules* **2014**, 19(12), 20325-20339.

120. Rahdar, A.; Taboada, P.; Aliahmad, M.; Hajinezhad, M. R.; Sadeghfar, F. Iron oxide nanoparticles: Synthesis, physical characterization, and intraperitoneal biochemical studies in Rattus norvegicus. *J. Mol. Struct.* **2018**, 1173, 240-245.

121. Kim, N.H.; Kim, J.-Y.; Ihn, K. J. Preparation of silver nanoparticles having low melting temperature through a new synthetic process without solvent. *J. Nanosci. Nanotechnol.* **2007**, 7(11), 3805-3809.

122. Liang, T.; Zhou, D.; Wu, Z.; Shi, P. Size-dependent melting modes and behaviors of Ag nanoparticles: a molecular dynamics study. *Nanotechnology* **2017**, 28(48), 485704.

123. Khanna, P. K.; Singh, N.; Charan, S.; Subbarao, V. V. V. S.; Gokhale, R.; Mulik, U. P. Synthesis and characterization of Ag/PVA nanocomposite by chemical reduction method. *Mater. Chem. Phys*. **2005**, 93(1), 117-121.

124. Abdul Kareem, T.; Anu Kaliani, A. Synthesis and thermal study of octahedral silver nano-plates in polyvinyl alcohol (PVA). *Arab. J. Chem*. **2011**, 4(3), 325-331.

125. Alpsoy, A.; Yasa, S.; Gündüz, U. Etoposide resistance in MCF-7 breast cancer cell line is marked by multiple mechanisms. *Biomed. Pharmacother*. **2014**, 68(3), 351-355.

126. Kmiecik, S.W.; Krzyścik, M. A.; Filip-Psurska, B.; Wietrzyk, J.; Boratyński, J.; Goszczyński, T. M. Methotrexate and epirubicin conjugates as potential antitumor drugs. *Adv. Hyg. Exp. Med.* **2017**, 71, 618-623.

127. Kullberg, M.; Mann, K.; Anchordoquy, T. J. Targeting Her-2+ breast cancer cells with bleomycin immunoliposomes linked to LLO. *Mol. Pharm*. **2012**, 9(7), 2000-2008.

128. Memariani, T.; Hosseini, T.; Kamali, H.; Mohammadi, A.; Ghorbani, M.; Shakeri, A.; Spandidos, D. A.; Tsatsakis, A. M.; Shahsavand, S. Evaluation of the cytotoxic effects of Cyperus longus extract, fractions and its essential oil on the PC3 and MCF7 cancer cell lines. *Oncology Lett*. **2016**, 11(2), 1353-1360.

129. Tomankova, K.; Polakova, K.; Pizova, K.; Binder, S.; Havrdova, M.; Kolarova, M.; Kriegova, E.; Zapletalova, J.; Malina, L.; Horakova, J.; Malohlava, J. In vitro cytotoxicity analysis of doxorubicin-loaded/superparamagnetic iron oxide colloidal nanoassemblies on MCF7 and NIH3T3 cell lines. *Int. J. Nanomed*. **2015**, 10, 949.

130. Zhao, Y.; Jing, Z.; Li. Y.; Mao, W. Berberine in combination with cisplatin suppresses breast cancer cell growth through induction of DNA breaks and caspase-3-dependent apoptosis. *Oncology Rep*. **2016**, 36(1), 567-572.

131. Nikazar, S.;Sohrab Nikazar, Sivasankarapillai, V. S.; Rahdar, A.; Gasmi, S.; Anumol, P. S.; Shanavas, M. S. Revisiting the cytotoxicity of quantum dots: An in-depth overview. *Biophys. Rev*. **2020**, 12(3), 703-718.

132. Sakinah, S. A. S.; Handayani, S. T.; Hawariah, L. P. A. Zerumbone induced apoptosis in liver cancer cells via modulation of Bax/Bcl-2 ratio. *Cancer Cell Int*. **2007**, 7(1), 1-11.

133. Al-Abd, A. M.; Mahmoud, A. M.; El-Sherbiny, G. A.; El-Moselhy, M. A.; Nofal, S. M.; El-Latif, H. A.; El-Eraky, W. I.; El-Shemy, H. A. Resveratrol enhances the cytotoxic profile of docetaxel and doxorubicin in solid tumour cell lines in vitro. *Cell Prolif*. **2011**, 44(6), 591-601.

134. Wu, S.-B.; Pang, F.; Wen, Y.; Zhang, H.-F.; Zhao, Z.; Hu, J.-F. Antiproliferative and apoptotic activities of linear furocoumarins from Notopterygium incisum on cancer cell lines. *Planta Med*. **2010**, 76(01), 82-85.

135. Shokrzadeh, M.; Saravi, S. S. S.; Mirzayi, M. Cytotoxic effects of ethyl acetate extract of Sambucus ebulus compared with etoposide on normal and cancer cell lines. *Pharm. Mag*. **2009**, 5(20), 316.

136. Zhu, D.; Tao, W.; Zhang, H.; Liu, G.; Wang, T.; Zhang, L.; Zeng, X.; Mei, L. Docetaxel (DTX)-loaded polydopamine-modified TPGS-PLA nanoparticles as a targeted drug delivery system for the treatment of liver cancer. *Acta Biomater*. **2016**, 30, 144-154.

137. Rahdar, A.; Aliahmad, M.; Samani, M.; Heidari Majd, M.; Md. Abu Bin Hasan, S. Synthesis and characterization of highly efficacious Fe-doped ceria nanoparticles for cytotoxic and antifungal activity. *Ceram. Int*. **2019**, 45(6), 7950-7955.

138. Abdulkhaleq, L. A.; Assi, M. A.; Abdullah, R.; Zamri-Saad, M.; Taufiq-Yap, Y. H.; Hezmee, M. N. M. The crucial roles of inflammatory mediators in inflammation: A review. *Vet. World* **2018**, 11(5), 627.

139. Ibrahim, F.; Prihantono, P.; Ahmad, M.; Siagian, N. A., The Effect of Pagoda Leaves Extracts on the Level of IL-6 of Female Rats Induced by Staphylococcus Aureus. *Health Notions* **2018**, 2(5), 539-545.

140. Atzeni, F.; Masala, I. F.; Sarzi-Puttini, P. A review of chronic musculoskeletal pain: central and peripheral effects of diclofenac. *Pain Ther.* **2018**, 7(2), 163-177.

141. Urquhart, E. Central analgesic activity of nonsteroidal antiinflammatory drugs in animal and human pain models. *Semin. Arthritis Rheum*. **1993**, 23(3), 198-205.

142. Park, W.; Won Park, Oh, Y. T.; Han, J. H.; Pyo, H. Antitumor enhancement of celecoxib, a selective Cyclooxygenase-2 inhibitor, in a Lewis lung carcinoma expressing Cyclooxygenase-2. *J. Exp. Clin. Cancer Res*. **2008**, 27(1), 1-9.

143. Rahdar, A.; Hajinezhad, M. R.; Nasri, S.; Beyzaei, H.; Barani, M.; Trant, J. F. The synthesis of methotrexate-loaded F127 microemulsions and their in vivo toxicity in a rat model. *J. Mol. Liquids* **2020**, 313, 113449.

144. Ratan, Z.A.; Haidere, M. F.; Nurunnabi, M.; Shahriar, S. M.; Ahammad, A. J. S.; Shim, Y. Y.; Reaney, M. J. T.; Cho, J. Y. Green chemistry synthesis of silver nanoparticles and their potential anticancer effects. *Cancers* **2020**, 12(4), 855.

145. Tong, J.; Yu, Q.; Xu, W.; Yu, W.; Wu, C.; Wu, Y.; Yan, H. Montelukast enhances cytocidal effects of carfilzomib in multiple myeloma by inhibiting mTOR pathway. *Cancer Biol. Ther*. **2019**, 20(3), 381-390.